13930

N84-27353

NASA

Technical Memorandum 86114

A COMPARATIVE REVIEW OF BOW SHOCKS AND MAGNETOPAUSES

R. P. Lepping

APRIL 1984

National Aeronautics and
Space Administration

Goddard Space Flight Center
Greenbelt, Maryland 20771

A Comparative Review of Bow Shocks and Magnetopauses

R. P. Lepping

Laboratory for Extraterrestrial Physics
Goddard Space Flight Center
Greenbelt, MD 20771

April 1984

Preface

This document is an expanded summary of a 30 minute review talk, originally entitled "Bow Shock and Magnetopause Formation", presented at the Conference on Planetary Plasma Environments: A Comparative View at Yosemite, California, on January 30 - February 3, 1984. This version is considerably extended generally in detail of discussion. It contains a highly selective number of topics presented with the intention of giving a broad overview of what is presently known. Figures 18, 20, and 22, not presented in the talk, have been added for completeness.

Not all of the references listed at the end of the document are cited in the text. Some were included simply to add to the usefulness and completeness of the list. For the sake of readability, no references appear in the Introduction.

Introduction

Measurements in the plasma and magnetic field environments of all the planets from Mercury to Saturn have been made by U.S. and U.S.S.R. spacecraft over the last 2 1/2 decades. From these observations we know that all of these planets possess bow shocks and almost all possess magnetopauses. Since Venus does not have a measurable intrinsic magnetic field, the solar wind interacts directly with Venus' ionosphere. Venus may thus prove to be the only planet in the entire solar system without a magnetopause, making it the interesting exception, although at present Mars still remains a controversial case. Other solar system bodies of interest which are continuously or transiently immersed in the solar wind include the terrestrial Moon, Saturn's satellite, Titan, and of course comets. Since our Moon has neither a global intrinsic magnetic field nor an atmosphere, and therefore is capable of totally absorbing the impinging solar wind, it possesses neither a bow shock nor a magnetopause. Titan experiences various plasma interactions depending on its location at a given time (solar wind, magnetosheath or magnetosphere of Saturn), but when in the solar wind, the interaction is Venus-like. It is very unlikely that a comet could possess a conventional magnetopause, since it is unlikely that a dirty, usually outgassing (at least within several AU of the sun), snowball is capable of maintaining an intrinsic field; it may or may not have a bow shock depending on its ability to absorb the solar wind.

The characteristics of bow shocks of planets depend strongly on the ever-changing solar wind conditions and not as much on the properties of the obstacles themselves; they have approximately spherical sunward profiles independent of whether they are ionospheres, magnetospheres or induced magnetospheres. However, Jupiter's magnetosphere is so severely distorted (out of spherical shape) by internal plasma that it is perhaps an exception to this, in that its bow shock, as well as its magnetopause, apparently has a different shape in meridian plane projection from that in the ecliptic projection, the latter being probably blunter. With this one exception, the study of planetary bow shocks is a study of the solar wind. For example, the strength of the shock is determined by <u>upstream</u> magnetic field, temperature, velocity, and density conditions, and even the fundamental character of the

shock (perpendicular, oblique, pulsation) varies in local time from dawn to dusk, depending on the direction of the upstream magnetic field. The profiles of planetary bow shocks are usually well represented by hyperbolas which would not be the case if the obstacles-to-flow were sharp-nosed. Magnetopauses, being current sheets, are very different from bow shocks: while they also depend strongly on solar wind conditions, they tell much more about the obstacle.

The shape of a magnetopause or of any obstacle-to-flow will depend crucially on the detailed 3-dimensional pressure profile that it presents to the solar wind. Of the planets already visited apparently only Mercury, Earth, and Saturn depend almost exclusively on the planet's intrinsic magnetic field for standing off the solar wind. In these cases the stagnation point distance R_{SP} (the planetocentric distance of the magnetopause along the sun-planet line) is well-determined by the solar wind dynamic pressure balance with the planet's nearly dipolar field, yielding:

$$R_{SP} \propto \left(\frac{M^2}{NV^2}\right)^{1/6}, \qquad (1)$$

where M is the planet's dipole moment, N is the solar wind proton density, and V is the solar wind speed. Those planets not possessing a measurable magnetic field, or having a weak field (Mars), are expected to have a small R_{SP} in terms of body radii. See Table 1 for a comparison of R_{SP}, M, and body size for the various "planets". Jupiter is not only unusual with regard to its size, field strength and obstacle size (R_{SP}) but also because of the considerable amount of plasma contained in its magnetosphere which causes its magnetopause boundary to be much more flimsy than that of Mercury, Earth, or Saturn. Magnetopause boundaries in ecliptic plane projection have been modeled by segments of ellipses, matched appropriately to straight lines for the magnetotail boundaries, or by parabolas, but the latter give a rather poor match to tail boundaries.

The remainder of this document, consisting of 22 figures and (for most) extended captions, will review some of the specific properties of known planetary bow shocks and magnetopauses.

Table 1

"Planet"	Body Radius (R_B) (10^3 km)	Magnetic Moment, M (G CM^3)	R_{SP}+ (R_B)	R_{SP}+ (10^3 km)	Type*
Mercury	2.44	$(3-5)\times10^{22}$	1.5±0.2	3.7±0.5	MP
Venus	6.05	$< 4\times10^{21}$	∿1.04	∿6.3	IP
Earth	6.38	8×10^{25}	11	70	MP
(Moon)	1.74	$< 1 \times 10^{19}$	NA	NA	SB
Mars	3.39	$\lesssim 2.5\times10^{22}$	1.25±0.1	4.25±0.3	MP/IP?
Jupiter	71.37	1.6×10^{30}	80	6,000	MP
Saturn	60.33	4.3×10^{28}	22	1,300	MP
(Titan)	2.57	$< 5\times10^{21}$	∿1	∿ 2.6	IP
(Comet)	∿0.001	0 ?	----	0.001-10	CS

* Type of Obstacle Boundary: MP = magnetopause, SB = surface of body, IP = ionopause, CS = contact surface

\+ Stagnation Point Distance (R_{SP}) is planetocentric and is based on an average of observations or on a model estimate

Figure 1 Here we present an outline of the topics discussed in the review.

COMPARATIVE BOW SHOCKS AND MAGNETOPAUSES

- INTRODUCTION: S.W. INTERACTION
  - BASIC PROPERTIES
  - MP CURRENT SYSTEM
- SOLAR SYSTEM OVERVIEW
- COMETS (COMPARISON WITH PLANETS)
- MERCURY
- VENUS
- MARS

  COMPARISON WITH EARTH

  SUMMARY
- JUPITER
  - MP: SIZE, SHAPE, DYNAMICS
  - R_{SP} POWER LAW
- SATURN
- MP SURFACE WAVES: SATURN, EARTH
  - CHARACTERISTICS
  - MP THICKNESS

FIGURE 1

Figure 2 When the solar wind impinges on the approximately dipolar magnetic field of a magnetic planet the field lines of the planet are stretched out in the anti-solarward direction, possibly thousands of R_E (Earth radii = 6378 km) in the earth's case. The boundary of this obstacle to solar wind flow is called a magnetopause (MP), which is to a first approximation impermeable to the solar wind. Within the MP is the magnetosphere. There is some plasma entry into the magnetosphere, directly through the MP and via the polar cusp (PC), forming plasma boundary layers, shown in the figure as: the high latitude plasma mantle (PM), the front-side entry layer (EL), and (not shown) the low latitude boundary layer along the extended MP. There is also (not shown) boundary layer plasma just above and below the plasma sheet (PS) in the magnetotail. Since the solar wind is supersonic and usually superalfvenic, an upstream bow shock is formed. The MP is either a tangential discontinuity or a rotational discontinuity depending on circumstances (outside the scope of this talk) and is supported by a current system, which is shown modeled in the next figure (Olson, 1982).

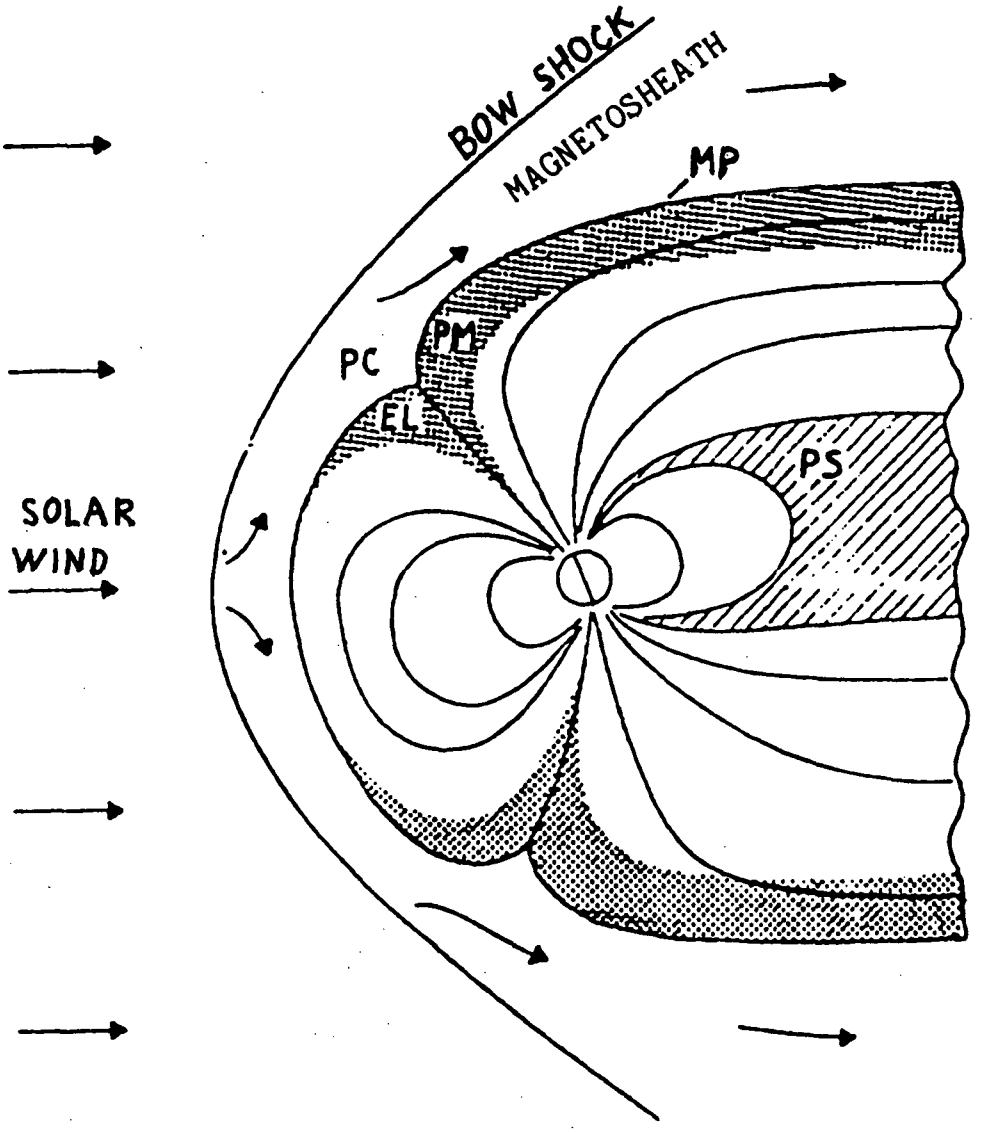

KEY:

EL - ENTRY LAYER

MP - MAGNETOPAUSE

PC - POLAR CUSP

PM - PLASMA MANTLE

PS - PLASMA SHEET

(PASCHMANN, 1979)

FIGURE 2

Figure 3 The right-hand side of the figure shows sketches of current systems which approximate those formed by the interaction of the solar wind with Earth's magnetic field (Olson, 1982). The top sketch shows the front side MP currents which flow eastward near the subsolar region and extend tailward near the flanks. Notice the dimple around the polar cusp. The bottom current system represents those associated with the magnetotail; these currents flow from dawn to dusk across the so-called neutral sheet (NS) and are diverted northward over the top lobe and sourthward around the bottom lobe, on the dusk side, in a nearly cyclindrical geometry. For completeness we show (center sketch) the ring current system which encircles Earth at a distance less than that of the front side MP currents, i.e., inside the magnetosphere. The sum of the magnetic fields resulting from these current systems should well approximate the net field due to the solar wind interaction, and that field added to the intrinsic field of the planet constitutes the total field of the magnetosphere.

On the left is shown a wire current loop model (Olson and Pfitzer, 1977) which represents an attempt to approximate the sum of the current systems shown on the right side of the figure.

[At this point Table 1 in the extended abstract (now in the Introduction) was discussed to give an overview of obstacle sizes, and type of obstacle boundary; the symbols under type are defined in the footnote to the table. Obviously the magnetic planets with the strongest dipole moments provide the largest obstacle sizes; this is dramatized in the next figure.]

WIRE CURRENT LOOP MODEL

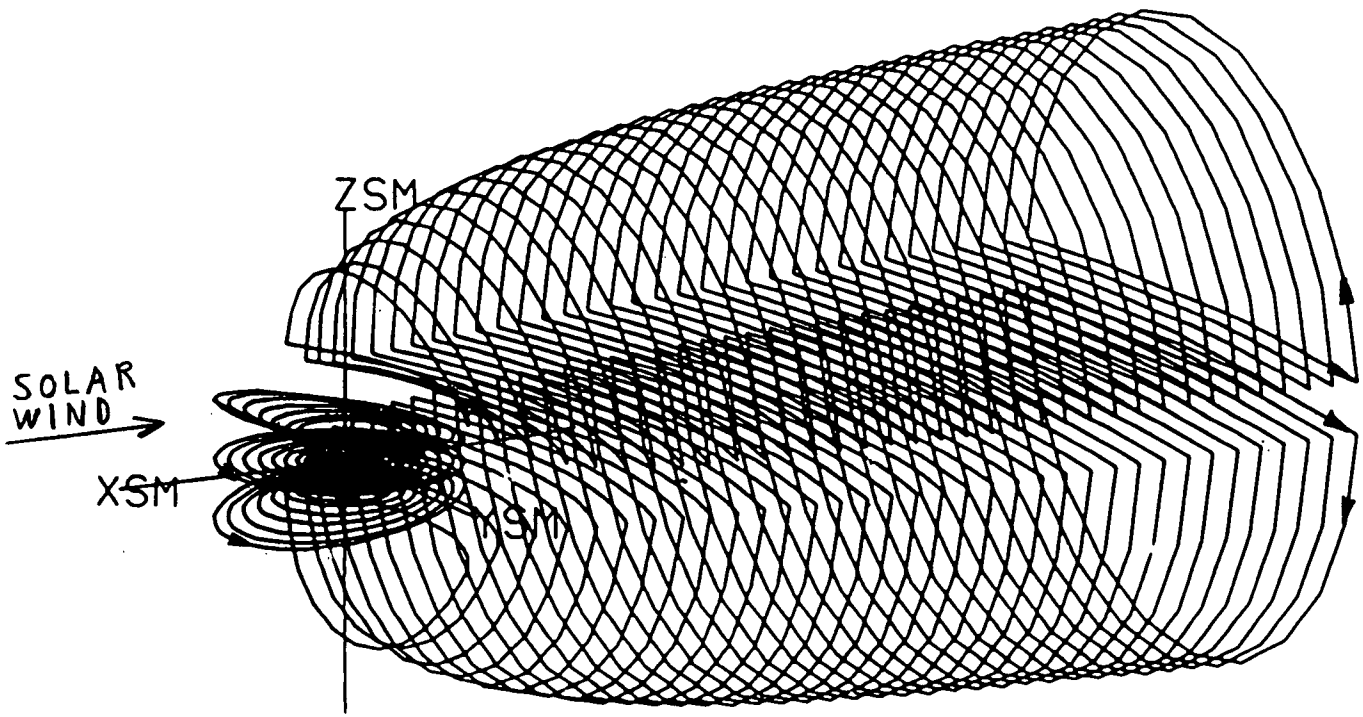

(OLSON AND PFITZER, 1977)

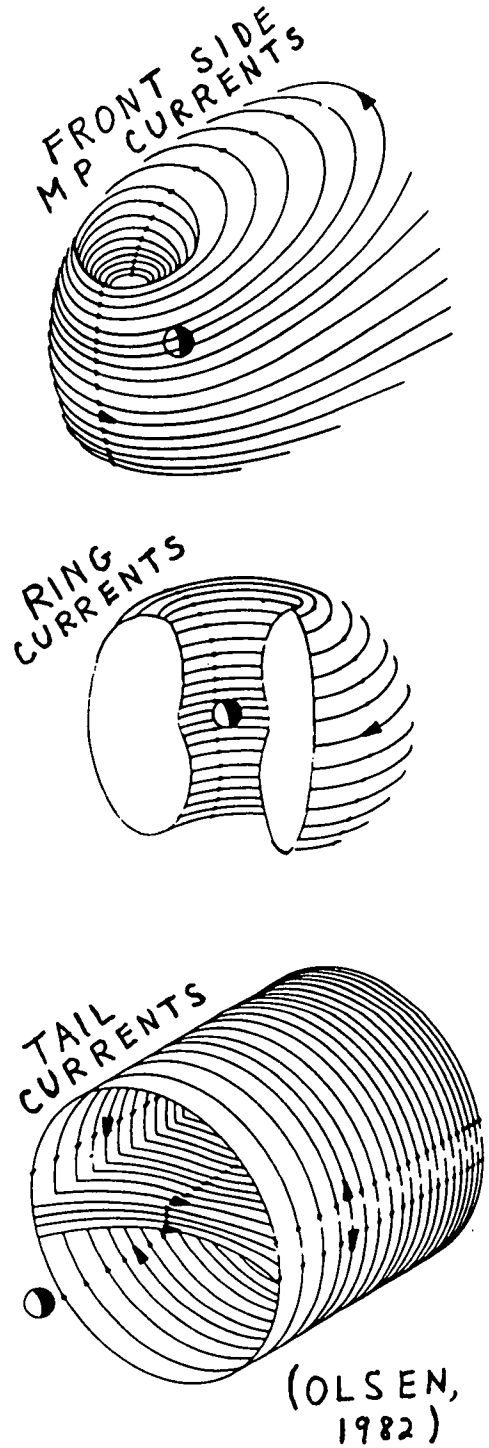

FIGURE 3

Figure 4 Shown is the stagnation point distance (R_{SP}), i.e., the planetocentric subsolar point distance, of the boundary of the various obstacles in the solar system. Notice that most of the known obstacle sizes cluster around an R_{SP} of 4,000 km. The R_{SP} for comets is not really known, but estimates put it in the range of $\sim$ 1 km to 10^4 km (Wilkening, 1982). R_{SP} for earth is significantly larger than that for the other terrestrial planets, and the known R_{SP} for the two giant planets, Jupiter and Saturn, dwarfs those of the terrestrial planets.

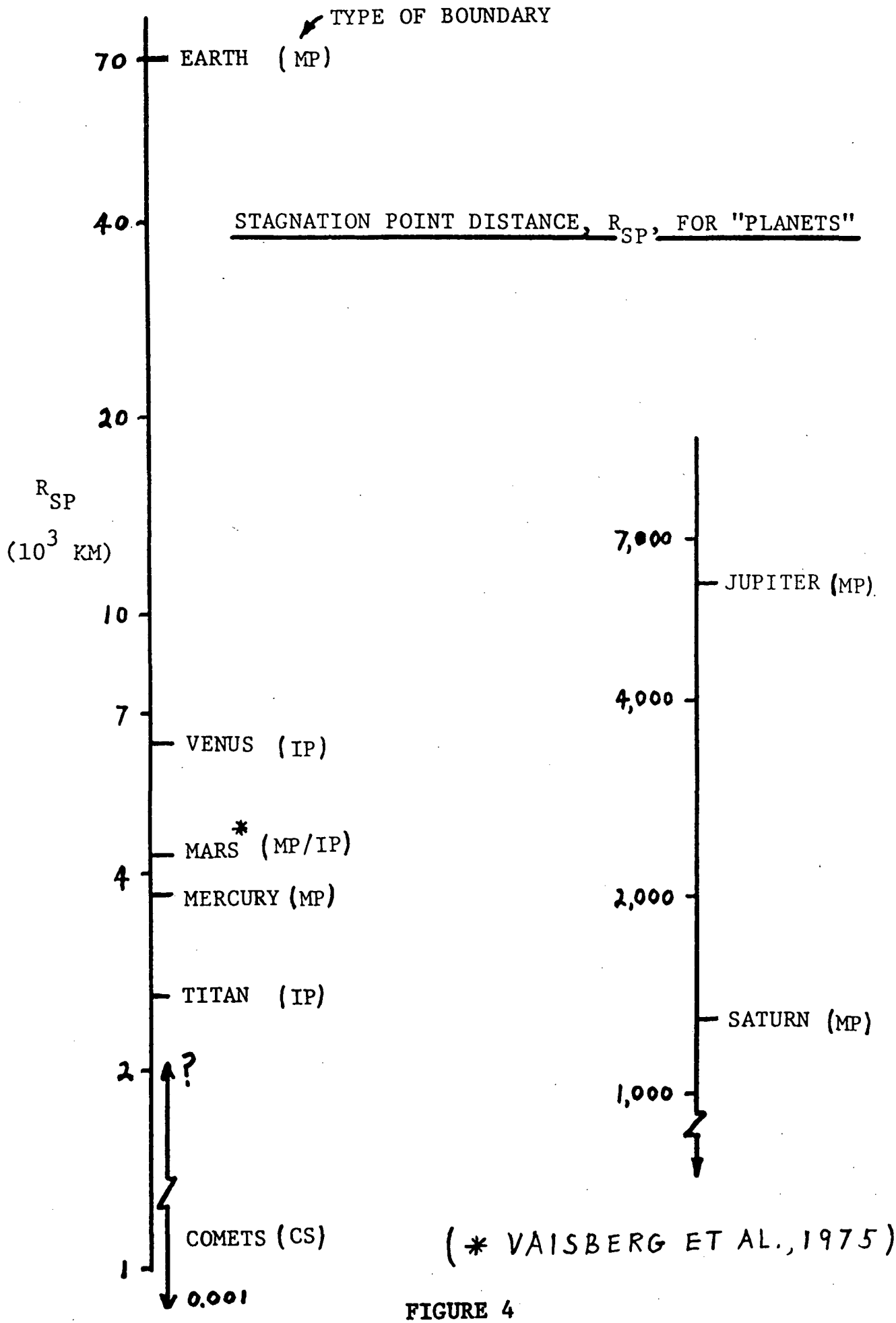
TYPE OF BOUNDARY
STAGNATION POINT DISTANCE, R_{SP}, FOR "PLANETS"
R_{SP}
(10^3 KM)
70
40
20
10
7
4
2
1
0.001
EARTH (MP)
VENUS (IP)
MARS* (MP/IP)
MERCURY (MP)
TITAN (IP)
?
COMETS (CS)
7,000
4,000
2,000
1,000
JUPITER (MP)
SATURN (MP)
(* VAISBERG ET AL., 1975)

FIGURE 4

Figure 5 We show this figure for a dual purpose: to describe possible solar wind comet interactions and to remind the reader of the occurrence of solar wind interactions in the solar system other than the earth-like one, i.e., one with an intrinsic magnetic field. At the top we show a lunar type of interaction of the solar wind with a nonmagnetic absorbing sphere (with an added tenuous atmosphere or without). This is a weak cometary interaction, implying small gas production as is usually characteristic of short period comets, or even of large comets at large distances from the sun. The middle sketch shows a solar wind Venus type of interaction in which the atmosphere/ionosphere is sufficiently dense to deflect the solar wind and create an upstream bow shock. (The interaction of the solar wind with Titan should resemble this case.) The obstacle in this case marginally stands off the solar wind, and a thick sheath is formed. However, an important difference between the Venus-like cometary interaction and the actual solar wind-Venus interaction is that gravity is important in the latter but negligible for a cometary interaction with the solar wind. The bottom example, a "solar wind type" according to Ip and Axford (1982), is a strong interaction in which the solar wind interacts with a comet that has a sufficiently large gas production rate such that the outflowing gas attains a supersonic speed, forming an inner shock as well as the outer bow shock (Wallis and Dryer, 1976); this will be described more fully in the next figure. Halley's comet in the vicinity of the sun (say at $\sim$ 1AU) may be an example of such a case. Ip and Axford (1982) suggest the possibility that some comets, those capable of large outgassing near the sun, evolve through these three stages, "lunar", "Venus" and "solar wind", as they travel from the far reaches of the solar system to the vicinity of the sun. This idea is somewhat controversial and, in fact, Ip (private communication, 1984) now expresses doubts about it.

POSSIBLE S.W. - COMET INTERACTIONS

(IP AND IXFORD, 1982)

Lunar type

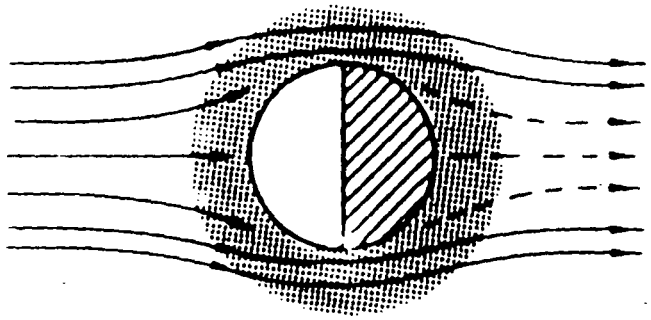

Venus type

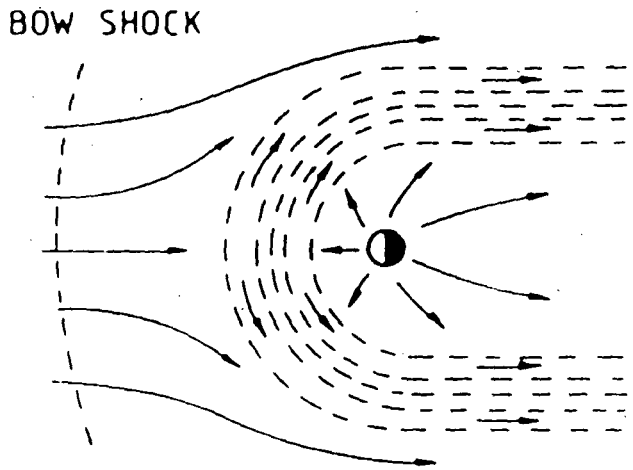

Solar wind type

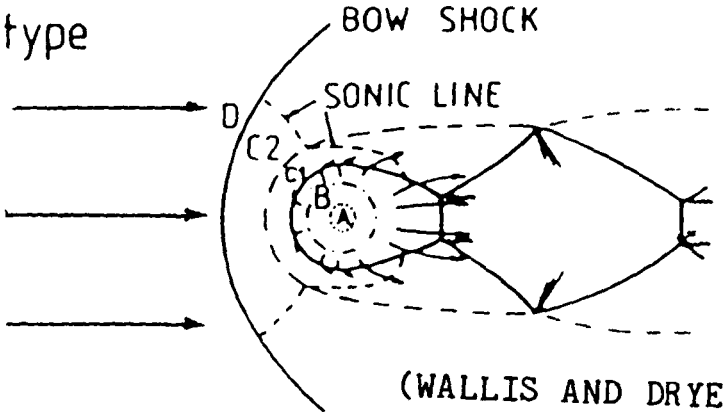

(WALLIS AND DRYER, 1976)

FIGURE 5

Figure 6 Here we briefly give a little more detail on the third type of comet interaction, as modeled by Wallis and Dryer (1976). First, it is assumed that the magnitude of the intrinsic or induced magnetic field of the comet is zero or negligible. As the comet approaches the sun and is heated, gas escapes, creating an envelope of subsonic source flow (A), and as the gas expands it goes supersonic (B) and passes through a boundary (Δ) where it becomes collision free. Also the gas becomes ionized, primarily by solar EUV, throughout region B. At the other extreme the solar wind (the exterior plasma) impinges on the cometary plasma and goes from supersonic to subsonic (C2), and therefore an upstream bow shock is formed, as shown in the figure. Likewise, the (interior) plasma of the comet environment goes from supersonic to subsonic (C1) creating an inner shock, as the figure also shows. The surface which separates the interior and exterior plasmas, i.e., the obstacle to solar wind flow, is expected to be initially a tangential discontinuity (TD), relaxing downstream to a contact discontinuity (D.A. Mendis, private communication, 1984); see the dashed MP-shaped surface in the figure. The expansion of the gas of the comet to a supersonic state is analogous to the same process of the solar wind near the sun, except that the sun's gravitational pull is replaced by the frictional drag of cometary dust particles in going from the solar process to the cometary one, according to Mendis.

POSSIBLE S.W. COMET INTERACTION

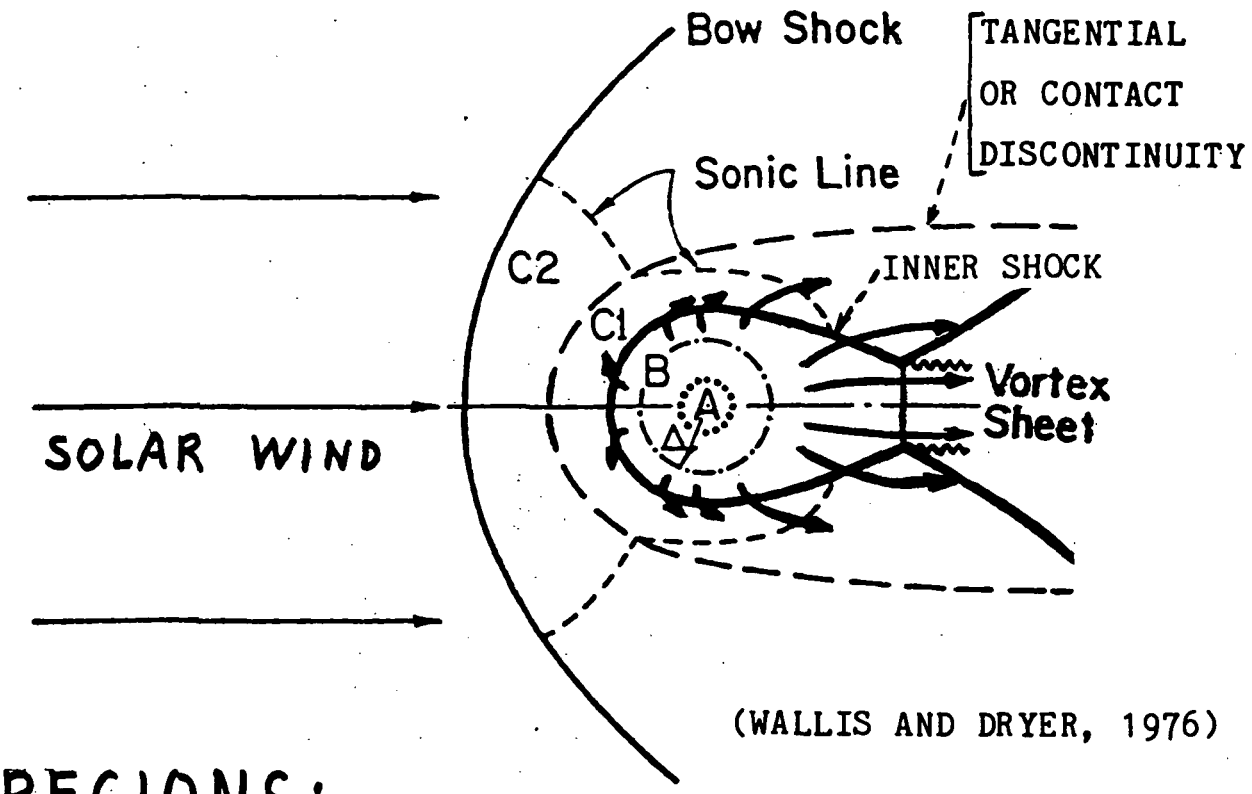

(WALLIS AND DRYER, 1976)

REGIONS:

A ___ SUBSONIC SOURCE FLOW

B ___ SUPERSONIC EXPANSION

C1 ___ SUBSONIC INTERIOR PLASMA

C2 ___ SUBSONIC EXTERIOR PLASMA

Δ ..... POSITION (CIRCLE) WHERE EXPANDING GAS → COLLISION-FREE

FIGURE 6

Figure 7 We now return to the interaction boundaries of the planets, starting with Mercury. Mariner 10 encountered Mercury three times over the years 1974-75, but we consider only the first (I) and third (III) encounters, because during the second encounter the spacecraft passed far in front of the planet, making that pass apparently useless for magnetospheric studies. In this figure we show the trajectory of Mariner 10 near Mercury in cylindrical coordinates for a 5° westward aberration (assuming solar wind [S.W.] flow radial) on the left side and for no aberration (assuming S.W. 5° from the east). Times in hours and minutes are marked on the trajectories, with pass I occurring on 29 March 1974, and pass III on 16 March 1975. The range of bow shock and magnetopause crossings are indicated on the figure. Shown also are the well-known Fairfield (1971) models for average bow shock and MP positions for earth's case scaled down to the size of Mercury's magnetosphere. Probably the No aberration case fits the model boundaries better than the 5° aberration case. The model MP's indicate that a planetocentric stagnation point distance of 1.45 R_M (radius of Mercury = 2435 km) is appropriate for these passes. Using the 1/6-th power law, given in the Introduction (Choe et al., 1973), along with R_{SP} = 1.45 R_M, suggests a planetary dipole moment of 5.6 x 10^{22} G cm^3, which agrees well (i.e., to within 10-20%) with the early harmonic expansion fits to the magnetospheric magnetic field data (Ness, 1976; Lepping et al., 1979); also see Table 1. One last remark: instead of the model bow shock fit shown here possibly a slightly blunter one would have fit better. This is consistent with the fact that blunter bow shock shapes are expected as the Alfvén mach number (M_A) is lowered (Rizzi, 1971), and for Mercury's distance from the sun M_A is $\gtrsim$ 4 $\leftrightarrow$ 6 typically, and for earth it is typically 7 $\leftrightarrow$ 9. We will discuss this point further when the work of Spreiter and Rizzi (Figure 12) is discussed.

MARINER 10 AT MERCURY, 1974 - 75

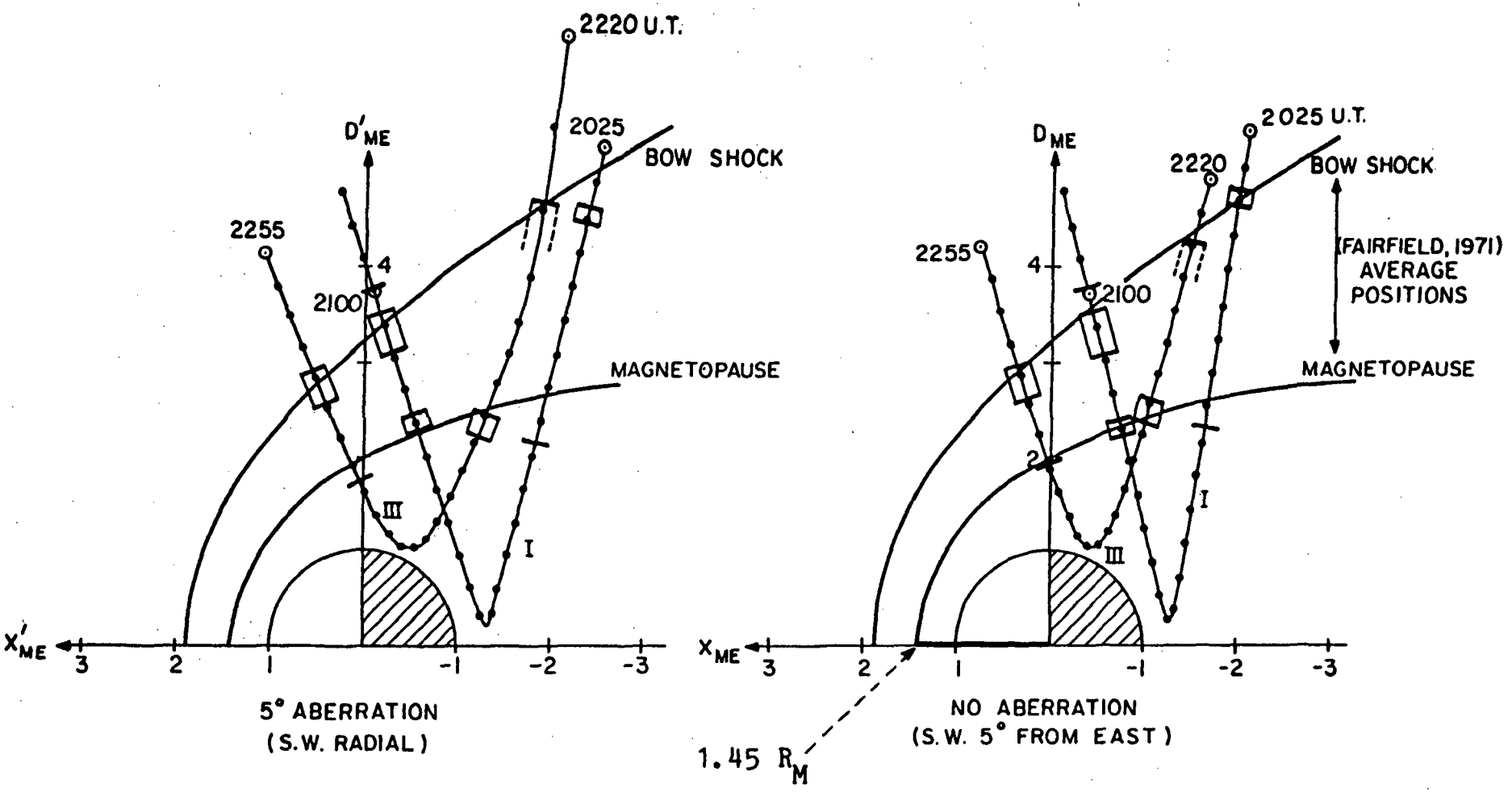

(LEPPING ET AL., 1979)

FIGURE 7

Figure 8 This and the next three figures deal with the work of Slavin and Holzer (1981). They have shown that a simple three parameter conic fit can satisfy observations for the bow shocks of the terrestrial planets where the form of the equation (2nd order polynomial) is shown in the figure, and where L is the semi-latus rectum, ϵ is the ellipticity, and X_0' is the position of the focus. The equation is restricted to the region $X' \geq -R_{OB}$, the obstacle radius, and the prime on X means that a transformation was carried out to a coordinate system in which aberration due to planetary motion approximately perpendicular to the solar wind flow direction has been removed. Slavin and Holzer perform "best-fits" of this equation to the frontside regions of the gas dynamic bow shock models of Spreiter et al., (1966) and Spreiter and Stahara (1980) for the earth's and Venus' cases, where the figure in the upper right hand corner shows the fits, and the points denoted by (+) were selected from the gasdynamic models used in the fits, all in cylindrical coordinates. The models were carried out for $M_S = 8$ and $\gamma = 5/3$ as shown, and the resulting three fit parameters are also displayed. Notice that Earth's bow shock is blunter than Venus' as indicated by the difference in the L's primarily. Also notice the difference in the focus positions: 0.25 R_{OB} for Earth and 0.45 R_{OB} for Venus. Now compare these model fits with similar conic fits made to actual data. The upper left hand corner shows the Venus bow shock crossings from Venera 9 and 10 (1975-6) data and the best fit curve and related parameters; N is the number of points used in the fit. First we notice that all fit parameters more closely match the earth's gasdynamic model than Venus'; in particular, L (1.95 R_V) is much larger than predicted (1.45 R_{OB}, where R_{OB} for Venus is not significantly larger than 1 R_V). Also notice that the bow shock sub-solar point is $\Delta \approx 1/4\ R_V$, not 1/2 R_V as had been predicted earlier. C.T. Russell (private communication, 1983) ascribes these effects to the fact that more S.W. is absorbed by Venus' atmosphere by charge exchange processes between the S.W. and the ionosphere than had been expected earlier. The figure in the bottom left shows the conic fit to Mars' bow shock observation based on the Soviet "Mars" spacecraft. Notice the similarities between the Venus and Mars fits for L and ϵ

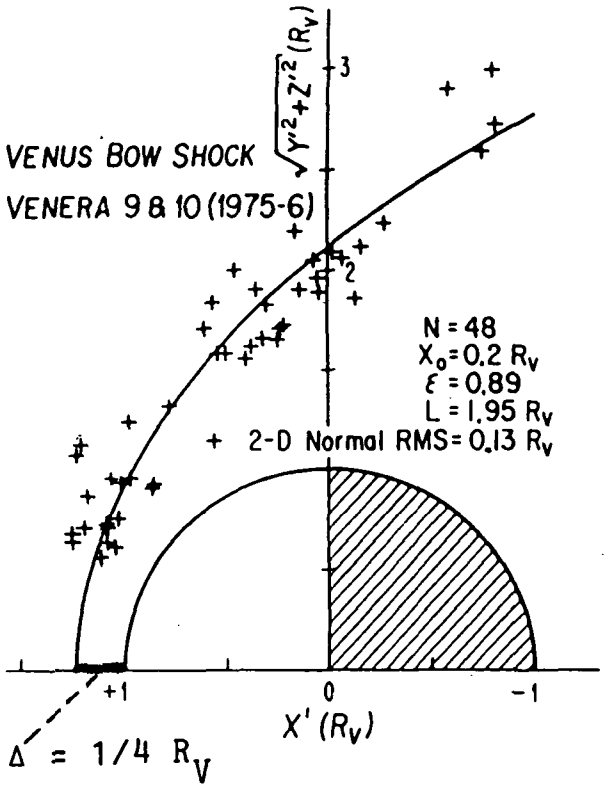

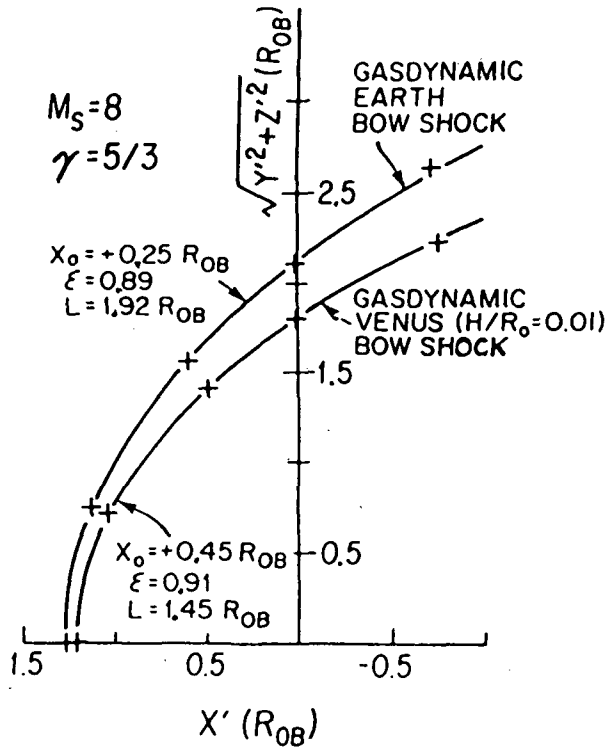

(SPREITER ET AL., 1966)

(" AND STAHARA, 1980)

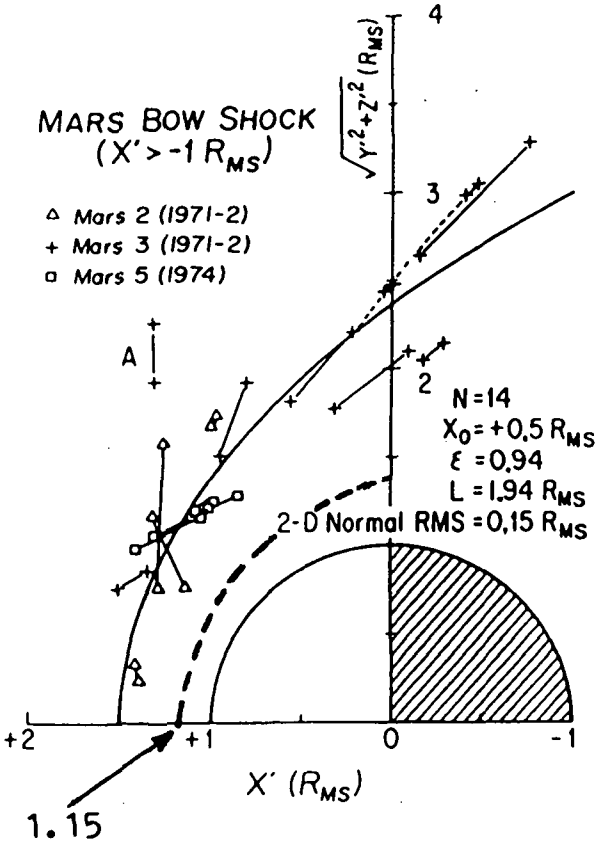

(SLAVIN AND HOLZER, 1982)

FIT EQUATION:

$r = L\,(1 + \varepsilon \cos\theta)^{-1}$

RESTRICTED TO REGION:

$X' \geq -R_{OB}$

X_0' IS FOCUS

AND PRIMED SYSTEM DENOTES ABERRATION IS ACCOUNTED FOR.

(SLAVIN AND HOLZER, 1981)

FIGURE 8

but the significant difference in the values for X_0': 0.2 R_V vs. 0.5 R_{MS}. This is indicative of a larger R_{SP} for Mars than Venus, with respect to R_{OB}, according to the authors. They interpret the obstacle for Mars in terms of an intrinsic field. In this regard we show their estimate of Mars' MP position and shape on this figure as a dashed curve (Slavin and Holzer, 1982).

A final point: in each of the conic fits ε was less than one indicating (a portion of) an ellipse, which has been used commonly in the past for fitting MP's! However, the authors point out that if downstream data (i.e., $X' < -R_{OB}$) had been included in the bow shock fits the resulting curves would be hyperboloids, also commonly used in the past for bow shocks.

Figure 9 Here Slavin and Holzer (1981) compare shapes and sizes of the bow shocks for the terrestrial planets in cylindrical coordinates. First we should point out, as briefly discussed in the Introduction, that a bow shock's shape is dependent on the shape of the obstacle to flow (more on this in Figure 13) and on upstream conditions, via M_S and M_A. Since the obstacles provided by Earth, Venus, and Mars are to a good approximation spherical, the differences in their bow shock shapes tell us something about differences in upstream conditions at their locations in the S.W. In the upper figure the conic model curves are plotted so that they share a common subsolar point - to compare shapes. This shows that Earth's bow shock is most blunt and Mars' bow shock least blunt; this will be discussed below (Figure 13). We point out however that the error-bars for the models of Venus' bow shock and those of its neighbors show considerable overlap. The bottom figure compares the sizes of the terrestrial bow shocks by plotting them in terms of planetary radii, R_P, where all were scaled to that value of solar wind dynamic pressure (shown in parentheses in the figure) which holds for Mars' case adjusted to 1AU. This figure is somewhat reminiscent of Figure 4.

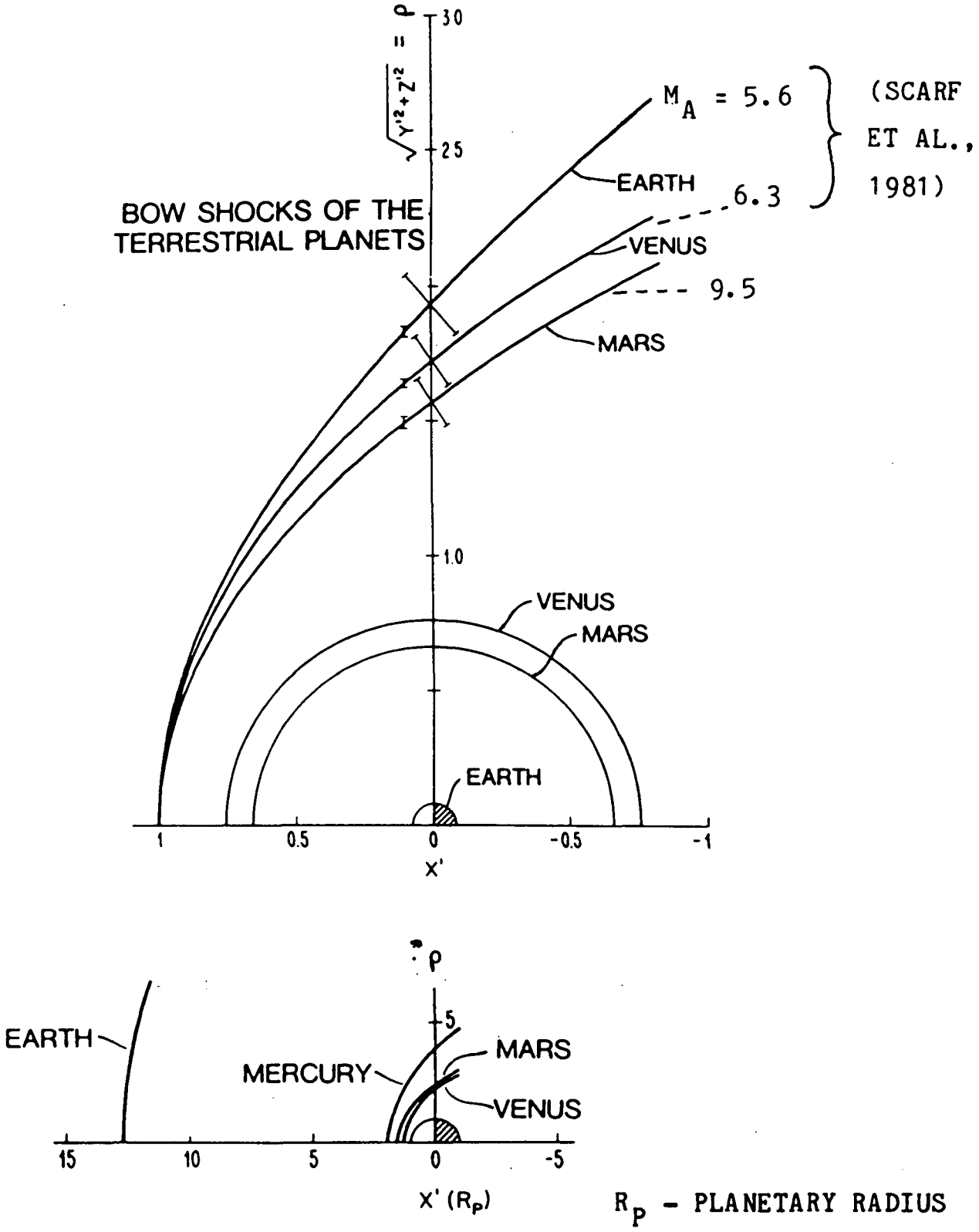

(SCALED TO P_{SW}=3.5×10^{-8}dynes/cm^2 at 1 AU)

(SLAVIN AND HOLZER, 1981)

FIGURE 9

Figure 10 Slavin and Holzer (1981) also discuss the cross-sectional shapes of the bow shocks of earth and Venus in the terminator plane. It was suggested by Cloutier (1976) and others that a bow shock may be oval in cross-section, with the oval's long axis perpendicular to the direction of $\vec{B}$(IMF) projected into the cross-sectional plane. The prediction was based on the expected anisotropic propagation of the shock wave with respect to the upstream $\vec{B}$. In the top of Figure 10 the location of Venus' bow shock (for N=17 crosssings) from the work of Romanov et al. (1978) based on data from Veneras 9 and 10 is shown as a dashed curve; Y'' is aligned with the projected $\vec{B}$(IMF), and aberration due to planetary motion has been removed in this system. The results appear to confirm Cloutier's prediction. Slavin and Holzer (1981) reexamined this issue by looking at a large number (N=172) of Pioneer Venus Orbiter (PVO) bow shock crossings and obtained an approximately circular cross-sectional shape for Venus' bow shock, shown by the heavy curve in the figure, indicating that this shape is apparently independent of $\vec{B}$(IMF), which contradicts the earlier results. (Also see Tatrallyay et al., 1983.) They repeated this work for Earth's case using IMP-4 data for N=69 crossings, also shown in the figure (light solid curve), and again obtained an approximately circular shape.

Since we are discussing cross-sectional shapes of boundaries we take this opportunity to compare the above results with estimations of the cross-sectional shape of the MP at earth from two studies. Using Explorer 33 and 35 MP crossings in the earth's tail at distances of 50 to 70 R_E Behannon (1970) determined that the earth's MP at these distances is on average 23.8 R_E in radius but slightly oval, being longer along the north-south line than the east-west line; see the bottom right-hand figure. On the other hand, Scarf et al. (1977) obtain an approximately circular cross-sectional shape for the earth's tail at $\gtrsim$ 25 R_E with a hint that the east-west dimension is larger than the north-south one, but there was no data at the northern or southern extremes; they used data from the IMP-7 spacecraft. Therefore this question appears to remain unanswered.

BOW SHOCKS OF EARTH AND VENUS MAPPED INTO THE TERMINATOR PLANE

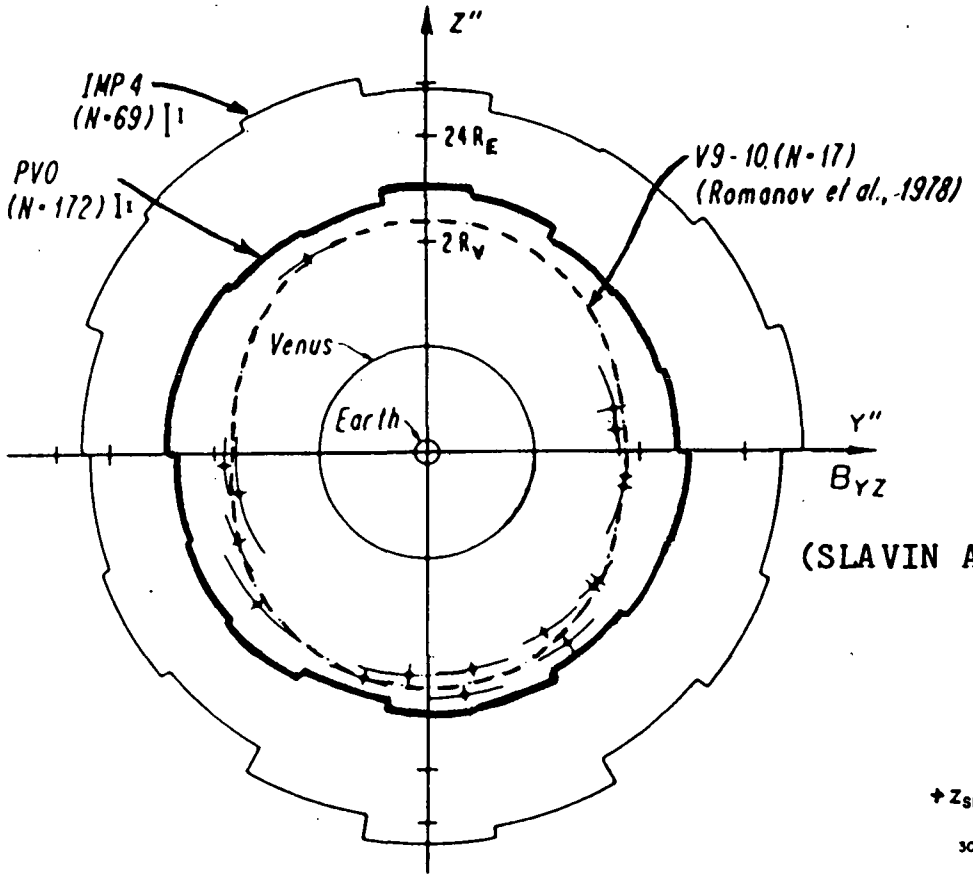

(SLAVIN AND HOLZER, 1981)

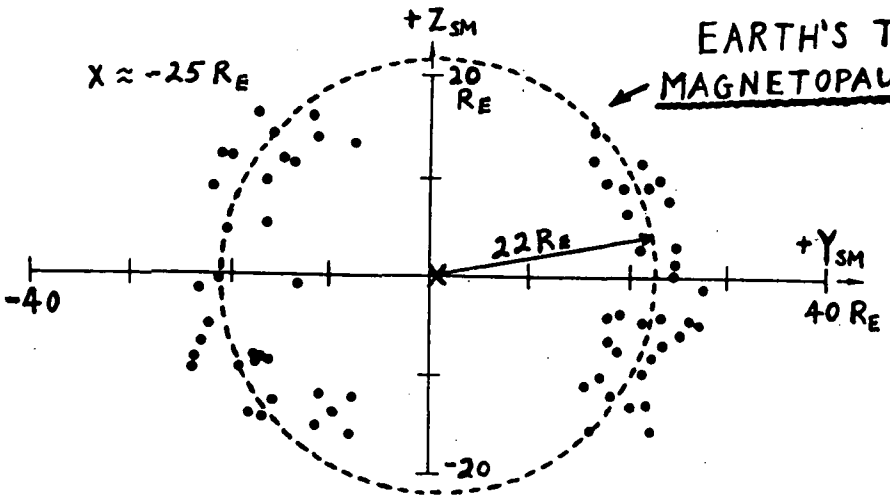

(SCARF ET AL., 1977)

EARTH'S TAIL MAGNETOPAUSE

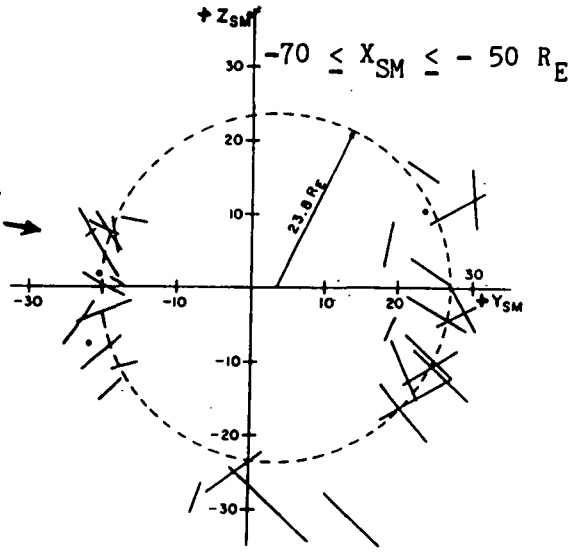

(BEHANNON, 1970)

FIGURE 10.

We should point out that all of these results, especially those on the MP shapes, are influenced (i.e., contaminated) by motions of the boundaries and probable size changes due to external pressure changes, since these were all single spacecraft studies.

Figure 11 In this figure we summarize some of the conclusions of Slavin and Holzer (1981). The parameters L, ε, λ, X_0', R_{OB} are defined in the caption of Figure 8, and M_{MS} is the magnetosonic Mach number.

MODELING BOW SHOCK POSITION AND SHAPE: THE TERRESTRIAL PLANETS

SLAVIN AND HOLZER (1981) CONCLUSIONS

- BS WELL FIT FOR VENUS, EARTH, AND MARS BY 3 PARAMETER CONIC MODELS:

  $r = L\ (1 + \varepsilon\ \cos\theta)^{-1}$, CENTERED AT FOCUS X_0', AND ABERRATED BY λ.

  — FOR $X > -R_{OB}$.

  AND $\varepsilon > 1$ ALWAYS FOR $X < -R_{OB}$.

- EARTH'S BS STAND-OFF DISTANCE, R_{SS} (SCALED BY $\rho\ V^2$) AND NEAR-PLANET SHAPE ORDERED BY M_S, NOT M_A OR M_{MS} — IN AGREEMENT WITH GAS DYNAMIC THEORY

- FOR TYPICAL S.W. CONDITIONS (I.E., NOT LOW M_A OR β) THERE IS NO EAST-WEST ASYMMETRY IN EARTH'S NEAR BS, AFTER ABERRATION CORRECTION.

- EARTH'S AND VENUS' BS SHOW NO SIGNIFICANT AXIAL ASYMMETRY IN TERMINATOR PLANE, I.E., NO SIGNIFICANT IMF DEPENDENCE.

- BLUNTNESS (b) OF BS FOR $X > -R_{OB}$:

  MARS: LEAST (ELLIPSOIDAL)
  VENUS: INTERMEDIATE (PARABOLOIDAL)
  EARTH: MOST (HYPERBOLOIDAL)

  } IN RESPONSE TO RESPECTIVE BLUNTNESS OF OBSTACLES

  WHERE $b = 1 - \varepsilon^2$ (VAN DYKE, 1958).
  AND ALL HYPERBOLOIDAL FOR DISTANT SHOCK.

FIGURE 11

Figure 12 We wish to develop a point referred to in the caption of Figure 7 about the importance of the Alfven mach number (M_A) under certain circumstances, i.e., when M_A is small (say <6 or so). Then point no. 2 in Figure 11 is not strictly correct. Spreiter has often (e.g., Spreiter, 1976) admonished those who incorrectly combined M_A and M_S into M^*, as shown in the figure, to form an "effective" mach number to replace M_S for the characteristization of the bow shock close to the ostacle. Changing M_S does not change the shape of the shock, only its position, but for a fixed M_S and for the upstream flow direction aligned with $\vec{B}$(IMF) as M_A gets smaller, as the figure shows, the bow shock gets blunter, i.e., it flares out on the flanks and gets closer at the sub-solar point. Possibly the ordering of the bluntness of the three bow shocks shown in Figure 9 is simply due to the influence of the interplanetary magnetic field. That is, the M_A's (upstream) at earth, Venus, and Mars are 5.6, 6.3, and 9.5, respectively, on average, according to Scarf et al. (1981), which give results that agree with the ordering in Figure 9 according to this concept. But, of course, upstream $\vec{V}_{SW}$ is not usually aligned with $\vec{B}$(IMF). The case for upstream flow perpendicular to $\vec{B}$(IMF) has not yet been computed.

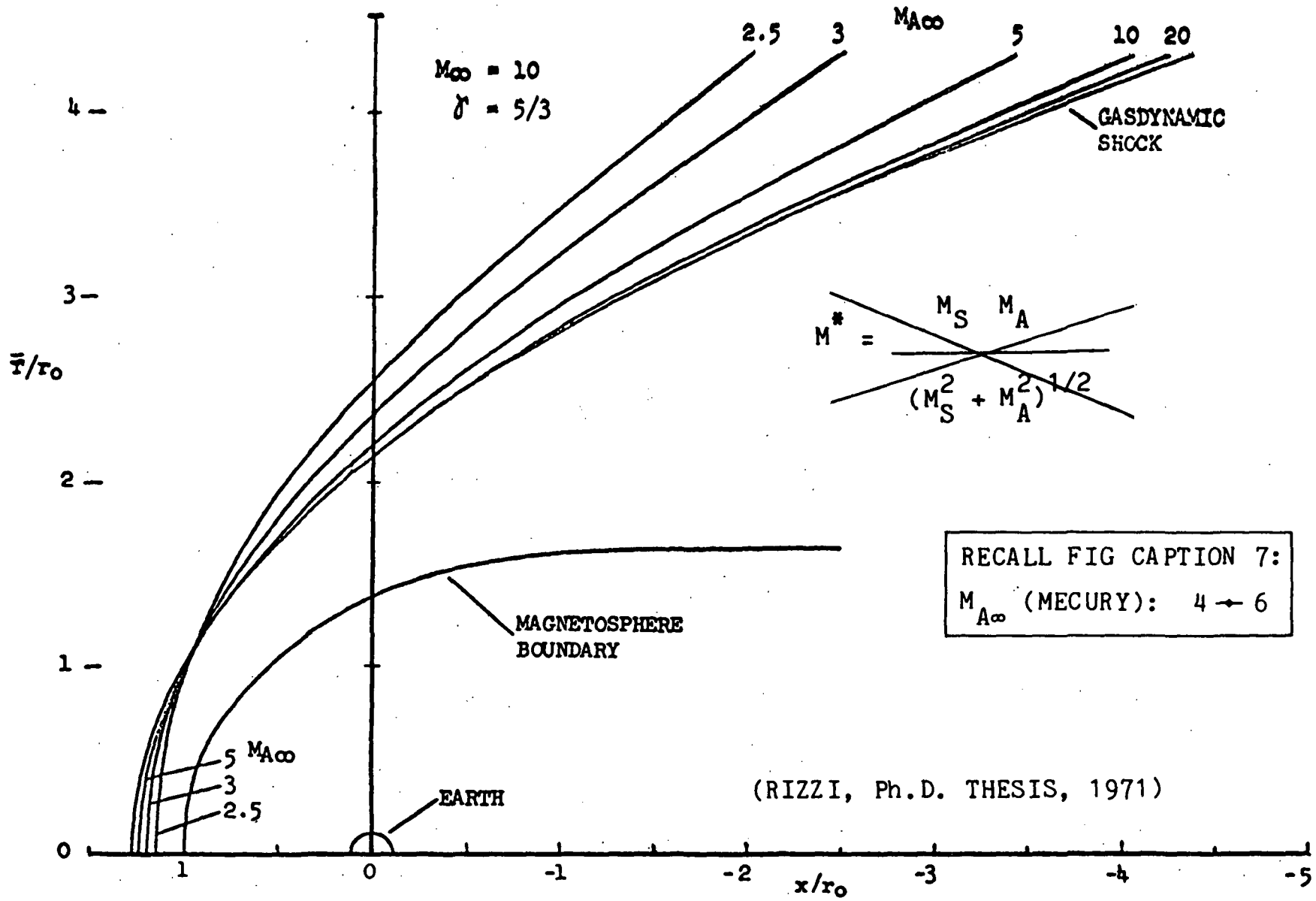
$M_\infty = 10$
$\gamma = 5/3$
$M_{A\infty}$
2.5
3
5
10
20
GASDYNAMIC SHOCK
$M^* = \frac{M_S \; M_A}{(M_S^2 + M_A^2)^{1/2}}$
RECALL FIG CAPTION 7:
$M_{A\infty}$ (MECURY): 4 → 6
MAGNETOSPHERE BOUNDARY
EARTH
(RIZZI, Ph.D. THESIS, 1971)
$\bar{r}/r_o$
x/r_o
4
3
2
1
0
1
0
-1
-2
-3
-4
-5

FIGURE 12

Figure 13 As we have seen, the shape of the bow shock can be influenced by the strength of M_A. The shape of the obstacle to flow can also help to determine the shape of the bow shock. Figure 13 shows two extreme cases: those of sharp nose (a) and blunt nose (b) obstacles. (These are not necessarily cylindrically symmetric obstacles.) In both cases, according to supersonic aerodynamic theory, the sheath thickness along the line of symmetry (denoted by Δ in the bottom part of the figure) is equal to 0.3 r_c, where r_c is the radius of curvature of the local part of the obstacle exposed directly to the flow; r_c is not necessarily dependent on the distance (R_{SP}) of the stagnation point from the planet (♃). The ratio $\Delta/\langle R_{SP}\rangle$ was calculated for the Earth's case from Fairfield's model (1971) and for Jupiter's case using observations from Voyager 1 (=0.26) and Voyager 2 (=0.22) from average boundary positions (Lepping et al., 1981). The overall average for Jupiter then is $\Delta/\langle R_{SP}\rangle = 0.24$. These are shown in the figure. Notice that Earth's case agrees well with theory implying a blunt obstacle (as we know it is, i.e., approximately a sphere). However, 0.24 for Jupiter implies a sharp nose obstacle. But Jupiter's magnetosphere is known directly from observations to be blunt-nosed in the ecliptic plane projection. Therefore, it must be sharp-nosed in the meridian plane projection. This conclusion is supported by Engle and Beard (1980), who derive a value of 1.6 for the maximum ratio of the long axis (d_{EQ}; equatorial) to the short axis (d_{N-S}; north-south) of the oval cross-section of the MP as projected into the terminator plane of Jupiter. We believe then that Jupiter's bow shock and MP in the vicinity of the planet have shapes like a "shark's head," resembling the top part (a) of Figure 13.

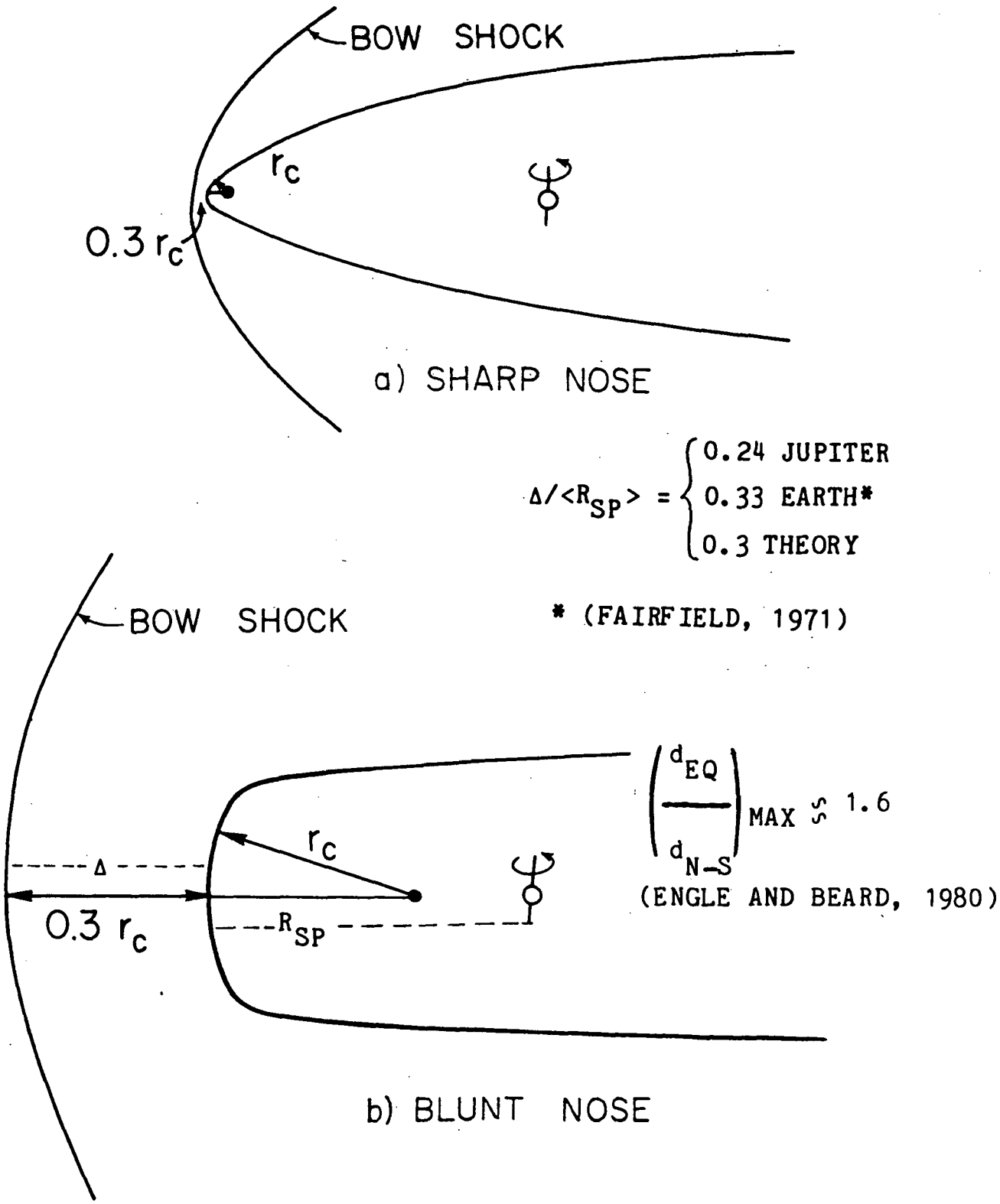

(COURTESY OF A. DESSLER, 1981)

FIGURE 13

Figure 14 We have used this idea of a shark's-head shape of Jupiter's frontside MP, coupled with that of the rocking motion of the magnetosphere (due to planetary spin and the angular offset of the planetary magnetic dipole axis of 9.6°), to explain observed large-scale variations of 5 and 10 hour quasi-periods of the magnetic field and plasma flow in the dawn magnetosheath (Lepping et al., 1981). The rocking motion of the MP is portrayed in the figure. These variations were observed by Pioneer 10 and Voyagers 1 and 2, and were most prominent in the north-south components of the B-field and the plasma velocity. This phenomenon was explained as the result of the 5 or 10 hour variation of interplanetary B-field line draping about the MP, and the concomitant solar wind plasma flow deviations, controlled by the periodic wobbling of the shark's-head MP. This periodic motion of field lines and plasma in the sheath caused large scale "tailward" propagating hydromagnetic waves to be generated whose speed with respect to the spacecraft was the sum of the convecting sheath plasma speed plus the wave speed in the plasma rest frame which was close to the Alfvén speed.

MODEL JOVIAN MAGNETOPAUSE

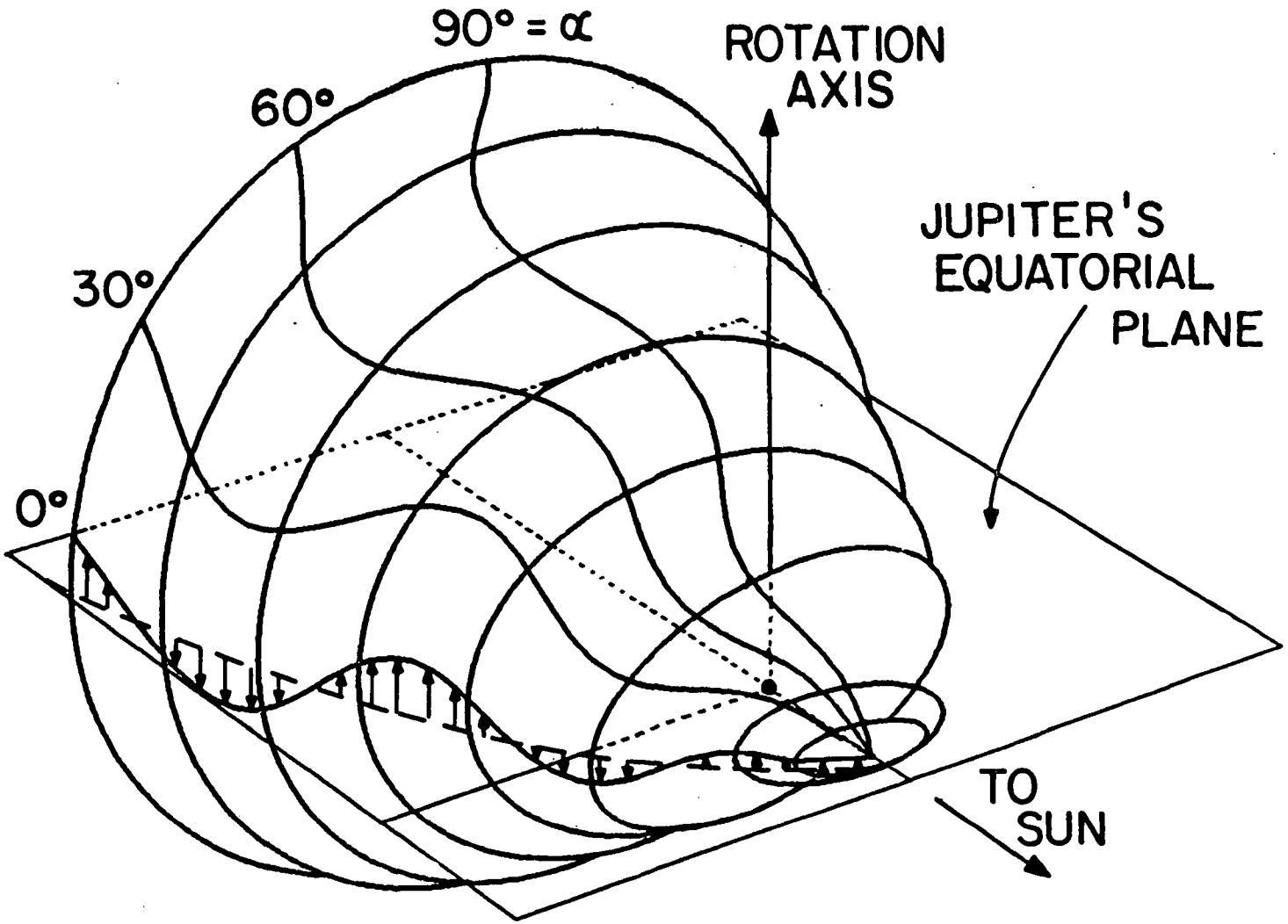

(LEPPING ET AL., 1981)

---- AVERAGE MAGNETOPAUSE POSITION IN EQUATORIAL PLANE

FIGURE 14

Figure 15 While we are talking about exotic shapes of MP surfaces, we show another unusual MP shape, to first order, that of the very large scale magnetotail of Jupiter as suggested by Lepping et al. (1983) which they assume extends approximately as far as the maximum length predicted by Grzedzielski et al. (1981), i.e., $\sim$15 AU. Lepping et al. predict that the shape should resemble a "string-of-sausages," because of the nearly 25-day periodic solar wind total pressure variation, which, according to Burlaga (1983) takes the form of non-linear corotating pressure waves at the distances from the sun of interest here, i.e., over at least the full length of Jupiter's tail. Between Jupiter and Saturn the tail should typically assume a minimum diameter $\lesssim$0.6 aU and a maximum diameter of $\sim$1.5 AU, and if the tail gets pinched off, a possibility suggested by Kurth et al. (1982), then the diameter would be zero AU, obviously. Lepping et al. also predict that the cross-section of the tail at any distance from Jupiter will very likely assume an oval shape (see upper right hand corner of the figure), because of the anisotropic contribution of the IMF pressure to the total external pressure exerted on the tail boundary under the conditions that the IMF possesses its most probable direction, that of being approximately in the ecliptic plane and nearly perpendicular to the radial direction (to the sun), and that the solar wind plasma-β at these distances is amaller than 1, 0.5 being a typical estimate. Michel and Dessler (1970) predicted such an oval cross-section for Earth's tail which may hold at great distances from Earth but not near the Earth where β is close to 1.

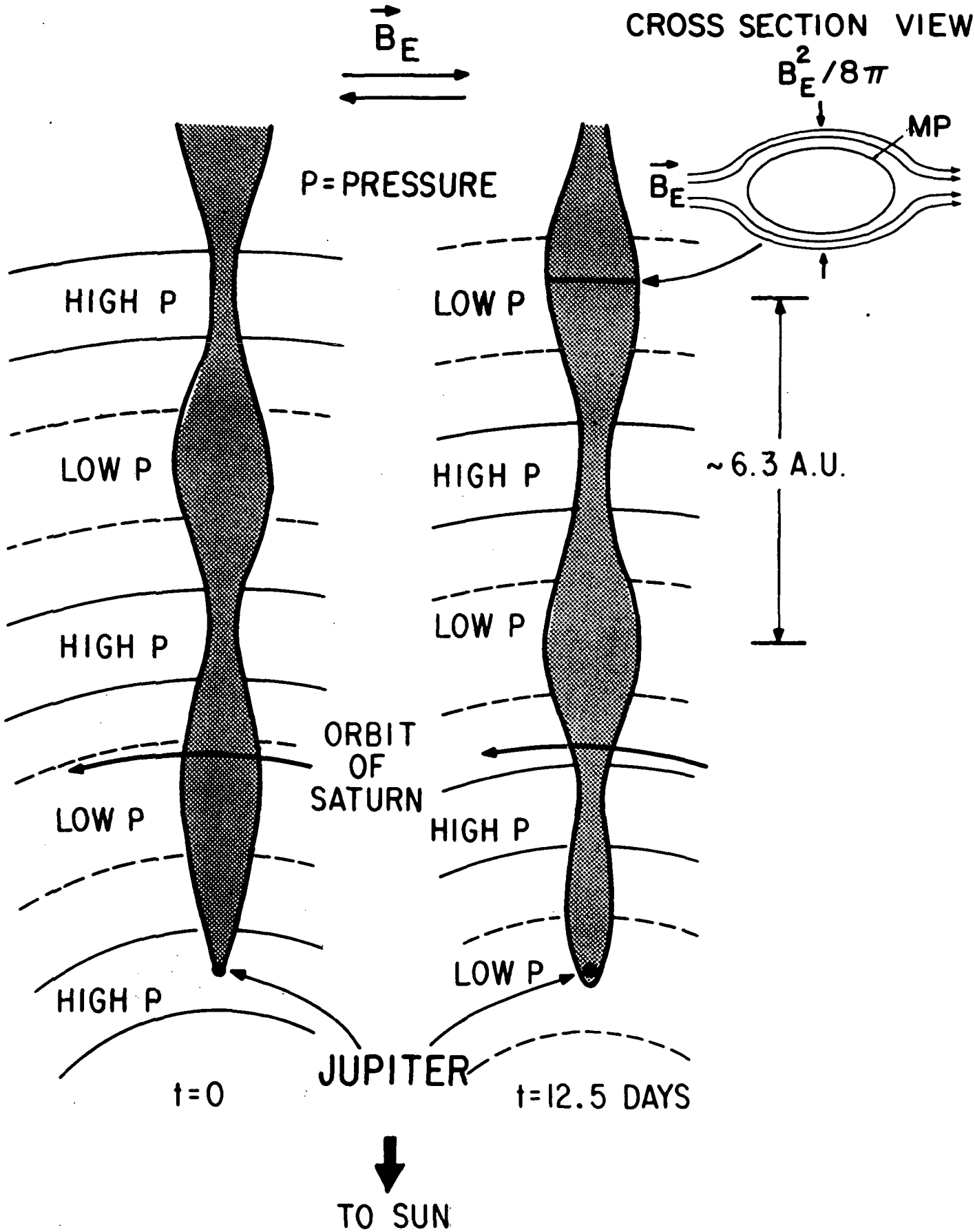

(LEPPING ET AL., 1983)

FIGURE 15

Figure 16 This figure and the associated work (Siscoe et al., 1980) nicely demonstrate how much more quickly the subsolar MP and bow shock boundaries of Jupiter respond to changing solar wind dynamic pressure, ρV^2, than the boundaries of the magnetospheres of the other known magnetic planets. This characteristic of Jupiter's magnetosphere is related to the shark's-head shape of the planet's MP (Figures 13 and 14) in that both the shape and flimsiness of the boundary are results of the unusually large amount of plasma in the equatorial region of Jupiter's magnetosphere. Siscoe et al. plot nV^2 against the subsolar distance (R_S) of the planet's bow shock using plasma data from Voyager 1 and 2. They assume that to first order the MP and bow shock move in unison and therefore, guided by the Earth's case, that $P \propto nV^2 = aR_S^{-b}$ for a and b unknown. To find values for a and b they perform least square regression analyses for the Voyager 1 and 2 data separately and for the alternate cases of the right-hand side of the equation as independent variable and vice-versa. They obtain values of b shown in the bottom-right portion of the figure, where a correlation coefficient of 0.9 was typical of all fits. Notice that b clusters around a value of 3 ($\langle b \rangle = 3.4$), whereas for Earth it is 6. (See our eq. 1 in the Introduction.) That is, R_S for Jupiter varies in response to changing solar wind dynamic pressure according to a 1/3-power law, and therefore Jupiter's front-side boundaries are flimsier than those of Earth. By taking the derivative of both sides of eq. (J-1) the authors obtain eq. (J-2), which gives an estimate of the shock speed in terms of (1/p) dp/dt. They estimate this quantity by using eq. (J-3), and for b they use the derived value of 3.

To obtain statistical properties of V_S, i.e., the average value and typical spread of V_S, they use 40 days of n and V data from Voyager 2 (from late December 1978 through early February 1979) for use in eq. (J-2), and determine that the average speed of the near subsolar bow shock, as encountered by the Voyager spacecraft, was 55 km/s. They argue that this high value for the approximate outward speed of the MP and bow shock may explain the observed sunward flow of plasma in Jupiter's magnetosheath for about 2 hours on one occasion (late on

SUNWARD FLOW IN JUPITER'S MAGNETOSHEATH

$$R_s = R_o\left(\frac{p}{p_o}\right)^{-\frac{1}{b}} \qquad \text{(J-1)}$$

$$\frac{dR_S}{dt} = V_s = -\frac{R_s}{bp}\frac{dp}{dt} \qquad \text{(J-2)}$$

$$\frac{\Delta p}{p\Delta t} = \frac{(nV^2)_1 - (nV^2)_2}{\frac{(nV^2)_1 + (nV^2)_2}{2}\,(4\text{ hr})} \qquad \text{(J-3)}$$

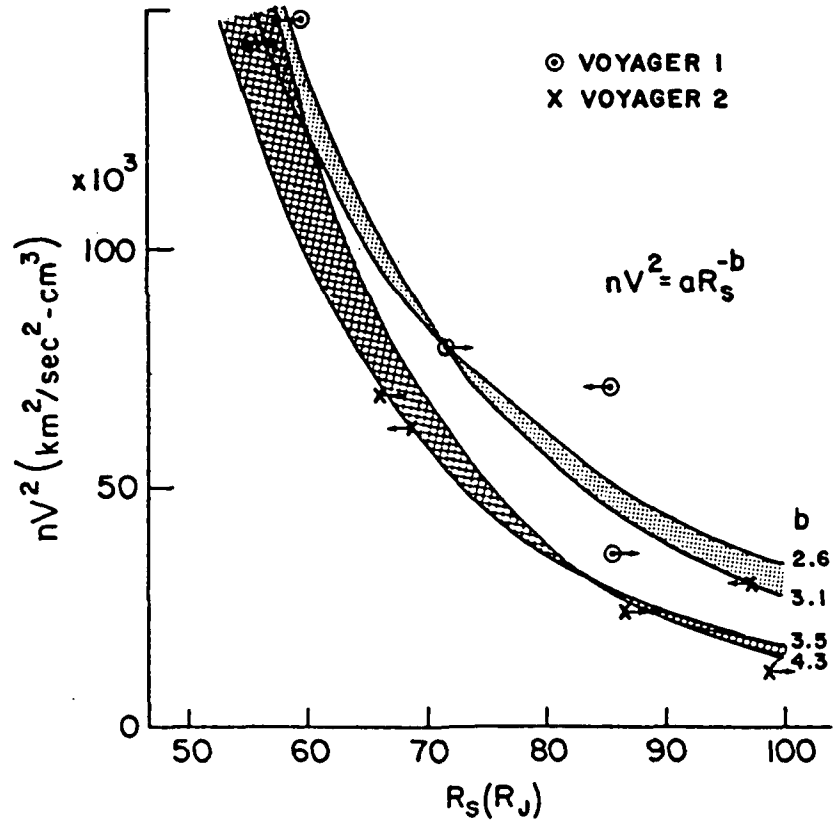

(SISCOE ET AL., 1980)

FIGURE 16

day 60, 1979; Voyager 2 data). The authors state that the effect of the expanding boundaries "...is like that of a snowplow of appropriately Olympian dimensions."

Figure 17 We now move on to Saturn and consider some work by Slavin et al. (1983) on the modeling of the planet's MP. They attempt to least-squares fit a curve to Pioneer 11 and Voyager 1 and 2 averages MP crossings by first scaling the averaged crossing positions according to an estimate of the solar wind dyanmic pressure, after accounting for the angle of attack of the solar wind to the boundary, Ψ_{MV}. The outbound Voyager 1 crossings were ignored because they occurred tailward of $X' = -R_{OB}$, violating the fit criteria. The form of the curve chosen for the fit is the same as that (conic) described in Figure 8 and repeated again in this figure, top right. At the top left, eq. (S-1) is the specific equation used for obtaining estimates of the solar wind dynamic pressure, P^*_{SW}, where Ψ_{MV} was obtained from minimum variance calculations of the magnetic field at the MP, and where B_{MP} is the field strength of the magnetosphere adjacent to the MP. Eq. (S-2) was used in each case to convert P^*_{SW} to an estimate of a normalized subsolar stagnation distance, R^*_N, by which the scaling was done. The figure on the left is the result of the fit where the crossing positions and fitted curve are put in cylindrical coordinates, $[(Y')^2 + (Z')^2]^{1/2}$ vs. X', and where the primes denote the fact that they are scaled quantities. All points were scaled to the value of P^*_{SW} shown in the figure. The fit-parameter values are also shown. Notice that ε is greater than 1 (1.09) which indicates that the curve is a hyperbola. This is unusual in that MP's of the other magnetic planets, in this projection, are well represented by parabolas or part of ellipses when the regions sunward of the planets are considered. The range of positions in real space coordinates (i.e., coordinates in which <u>no pressure scaling was done</u>) for the outbound Voyager 1 crossings (Bridge et al., 1981 and Ness et al., 1981) is shown in the figure and denoted V1; recall that these crossings were ignored in the curve-fitting by Slavin et al. (1983). No reasonable pressure scaling would put these crossings on the resulting curve; they <u>would</u> always fall significantly tailward of it.

SATURN MAGNETOPAUSE

THIS ASSUMES $P_{THERMAL}$ (IN) = 0

$$P^*_{SW} = B^2_{MP}/(8\pi\cos^2\psi_{MV}) \qquad \text{(S-1)}$$

THEN ASSUME THAT

$$R^*_N \sim (P^*_{SW})^{-1/6} \qquad \text{(S-2)}$$

(ADAPTED FROM SLAVIN ET AL., 1983)

$r = L\,(1 + \varepsilon \cos\theta)^{-1}$

$X' \geq -R_{OB}$

(SEE CAPTION TO FIG 8)

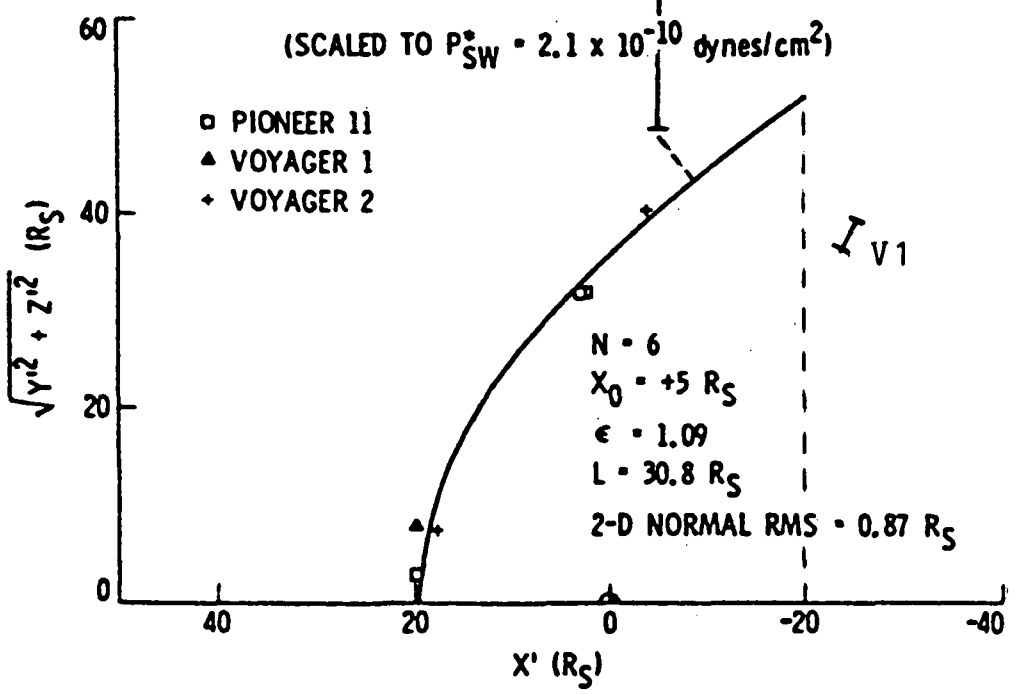

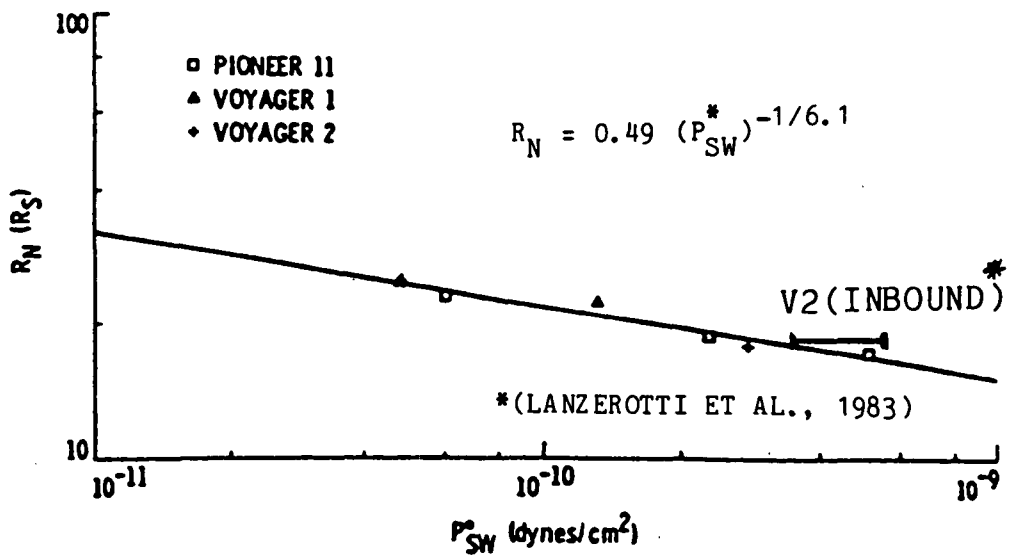

FIGURE 17

Hence, we believe that by ignoring these crossings the resulting curve became too blunt-nosed (hyperbola). Otherwise the model MP would have been closer to an earth-like shape (see Figure 18). We also point out that the actual (real space) range of outbound Voyager 2 MP crossings occurred over the region denoted by V2 (Bridge et al., 1982). Even after possible scaling of these crossing positions, the Slavin et al. average position (+) corresponds to the nearest outbound Voyager 2 crossings. The authors point out that they used only the nearest outbound Vaoyger 2 crossings, because it was the common subset of crossings that the plasma and magnetometer teams reported on (see Ness et al., 1982b). If, however, the unusually distant outbound Voyager 2 MP crossings were the result of Saturn's magnetosphere being in Jupiter's distant tail, as suggested by many studies (e.g., see Behannon et al., 1983, and Desch, 1983), then it is indeed best to ignore all of them, not just some of them as Slavin et al. did.

On the right-hand side of Figure 17 we show a figure from Slavin et al. (1983) which was used to demonstrate the relationship between R_N and P^*_{SW} where the internal thermal plasma pressure (P_{th}(in)) was assumed to be zero. In the figure these quantities are plotted for the same average crossings positions considered in the left-hand figure where now obviously no scaling was used. The authors mapped the averages of the actual crossing positions to the subsolar line and obtained R_N for each case which was plotted against P^*_{SW}, previously estimated, and the resulting points then were fit to a straight line in log-log space, yielding

$$R_N = 0.49\ (P^*_{SW})^{-1/6.1}.$$

This shows that Saturn's front-side MP responds similarly to Earth's with respect to solar wind dynamic pressure changes, i.e., according to the 1/6th power law. However, one cannot conversely conclude from this that the pressure just inside the front-side MP is always purely magnetic ($B^2/8\pi$) in character. Lanzerotti et al. (1983) show that the β of the plasma at times exceeded 1.0 and often exceeded 0.5

along Voyager 2's inbound trajectory just insider Saturn's MP. They suggest that by taking this into consideration a modification of the inbound Voyager 2 (R_N, P^*_{SW})-point in the figure should be made; actually they estimate a modified range, which is also shown in the figure. They point out that the straight line fit by Slavin et al. (1983) is obviously not very sensitive to this change, since the range lies close to their fitted-line, even though they assumed $P_{th}(in) = 0$. Therefore showing that $R_N \sim (P^*_{SW})^{1/6.1}$ for Saturn does not necessarily tell us that β is always low within the magnetosphere. By comparing Voyager 1 and 2 with respect to this question, Lanzerotti et al. (1983) conclude that the measured $\vec{B}$ just inside the Saturnian MP can be considered to arise principally from the planetary magnetic field. In the case of a greatly extended Saturnian MP the $\vec{B}$ at the boundary may consist of internal magnetosphere current systems as well.

Figure 18 Using similar techniques Slavin et al. (1983) model Saturn's bow shock, and they compare the bow shocks and MP's of Saturn and Earth in terms of obstacle radii (R_{OB}), where 1 R_{OB} = 10.3 R_E for Earth and 19.7 R_S for Saturn. Again they display the boundaries in cylindrical coordinates. It appears that the Saturnian bow shock is also excessively blunt in comparison to Earth's, and undoubtedly this is due to ignoring the Voyager 1 outbound crossings as well. One might consider how a Saturnian tail MP boundary having an approximately cylindrical shape (or, near Saturn, a cone shape of very small cone-angle) would match the MP shown in this figure. Obviously there would be a large discontinuous derivative (i.e., $d\rho/dX'$, where $\rho = [(Y')^2 + (Z')^2]^{1/2}$) at the connection line (a circle in 3-D) which is, of course, forbidden. As we see, Earth's case is well behaved, as expected. The terrestrial bow shock model of Slavin and Holzer (1981) and the terrestrial MP model of Holzer and Slavin (1978) were used in the comparisons.

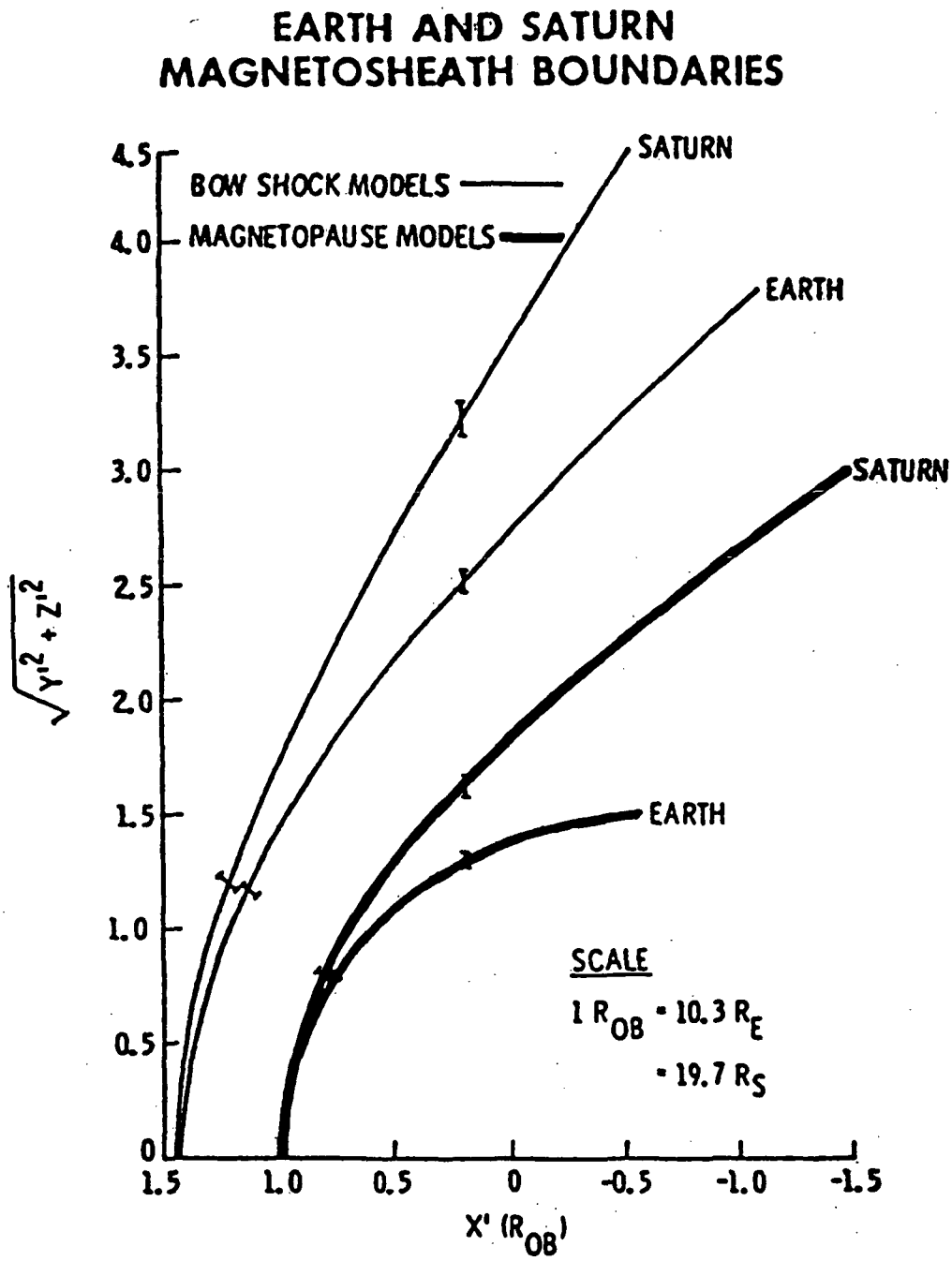

(SLAVIN ET AL., 1983)

FIGURE 18

Figure 19 While Voyager 1 was inbound toward Saturn near the subsolar line the spacecraft observed five quasi-periodic crossings of the MP suggesting that surface waves were occurring on the MP (Lepping et al., 1981). This was consistent with the fact that the solar wind was exceedingly steady and therefore bulk motion of the MP was not likely; the apparent distance from the single bow shock to the set of MP's, based on the spacecraft speed and times of occurrence, matched within about 20% an estimate of the subsolar magnetosheath thickness based on inbound and outbound crossings (Ness et al., 1981) implying a steady solar wind, at least inbound. In the upper left-hand corner of the figure the ecliptic plane projection of the spacecraft's trajectory near Saturn is shown. Magnetic field data is plotted in the figure in terms of the magnitude, B, and the heliographic longitude, λ, and latitude, δ, where $\lambda=0°$ is antisunward and $\delta=90°$ is "northward." The bow shock and MP crossings, MP (1 through 5), are clearly denoted in the figure and large field magnitude variations are seen in the magnetosheath; these were also briefly discussed by Lepping et al. (1981). Notice that the MP crossings had in all cases large angle changes allowing accurate estimation (through field variance analyses) of the normal to the boundary, which was also shown to be periodically varying as expected. Knowledge of the time durations between crossings, the spacecraft vector velocity, accurately determined normals at each crossing, and simple realistic assumptions allowed the authors to determine uniquely the basic characteristics (period, amplitude, wavelength, wave speed, etc.) of the surface waves. They assumed the waves were due to the Kelvin-Helmholtz instability (e.g., see Lee et al., 1981, and references therein) operating at the boundary and driven primarily by the much faster internal plasma of the magnetosphere.

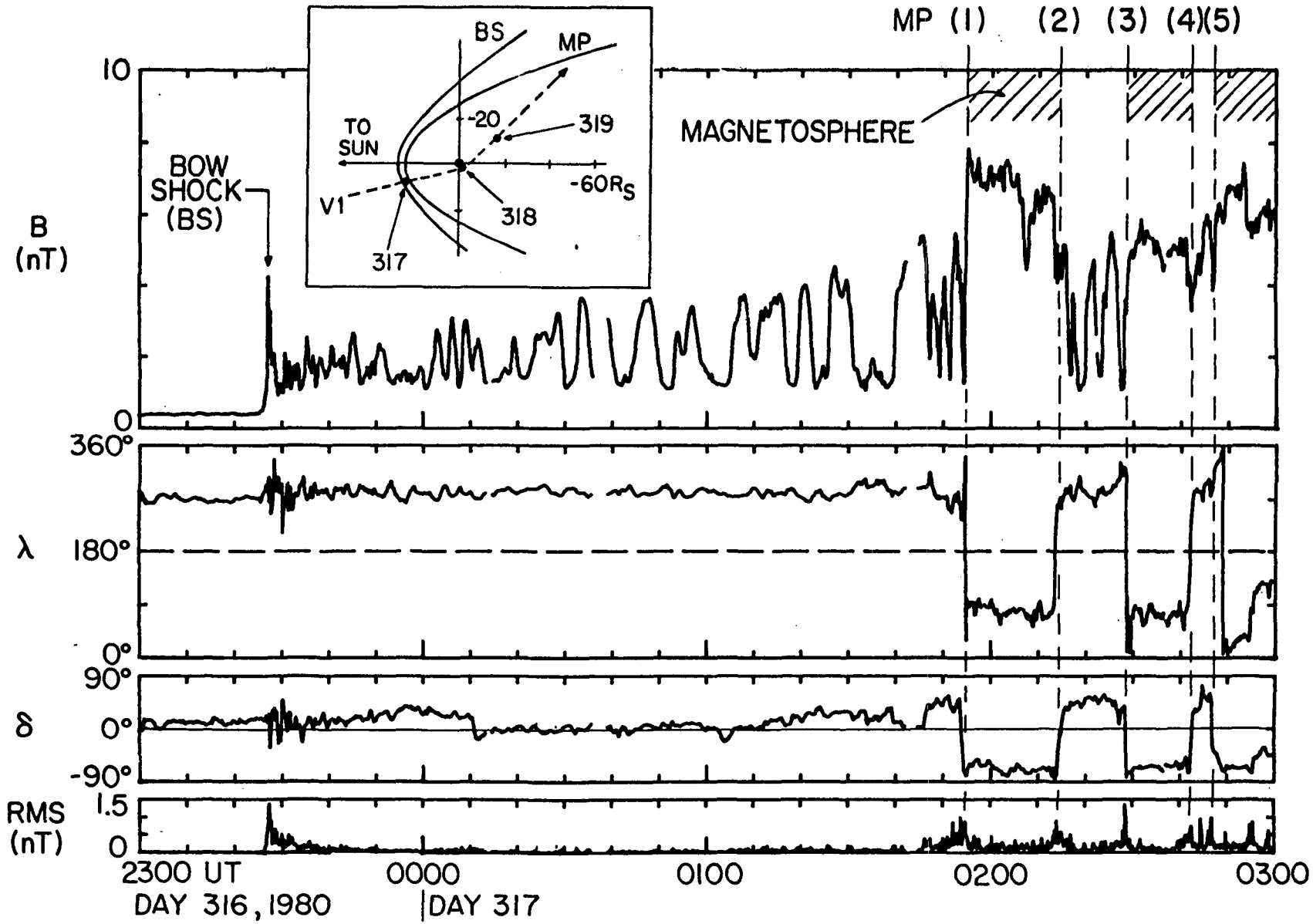

(LEPPING ET AL., 1981)

FIGURE 19

Figure 20 The crossings were used in sets of three (contiguous) for each calculation, yielding three parameter-set estimates. For example, this figure shows the results of the last set or case III (crossings: D3, D4, D5) drawn to scale, where X_{MP} is aligned with the MP, and Y_{MP} is perpendicular to it. The angle $\lambda_o = 197°$ refers to the fact that the unperturbed MP normal was 197° from the direction toward Saturn, measured clockwise, as shown at the bottom. As seen, the model allowed variable wavelength and amplitude over a cycle of the surface wave. The waves were determined to be moving tailward, approximately in the equatorial plane.

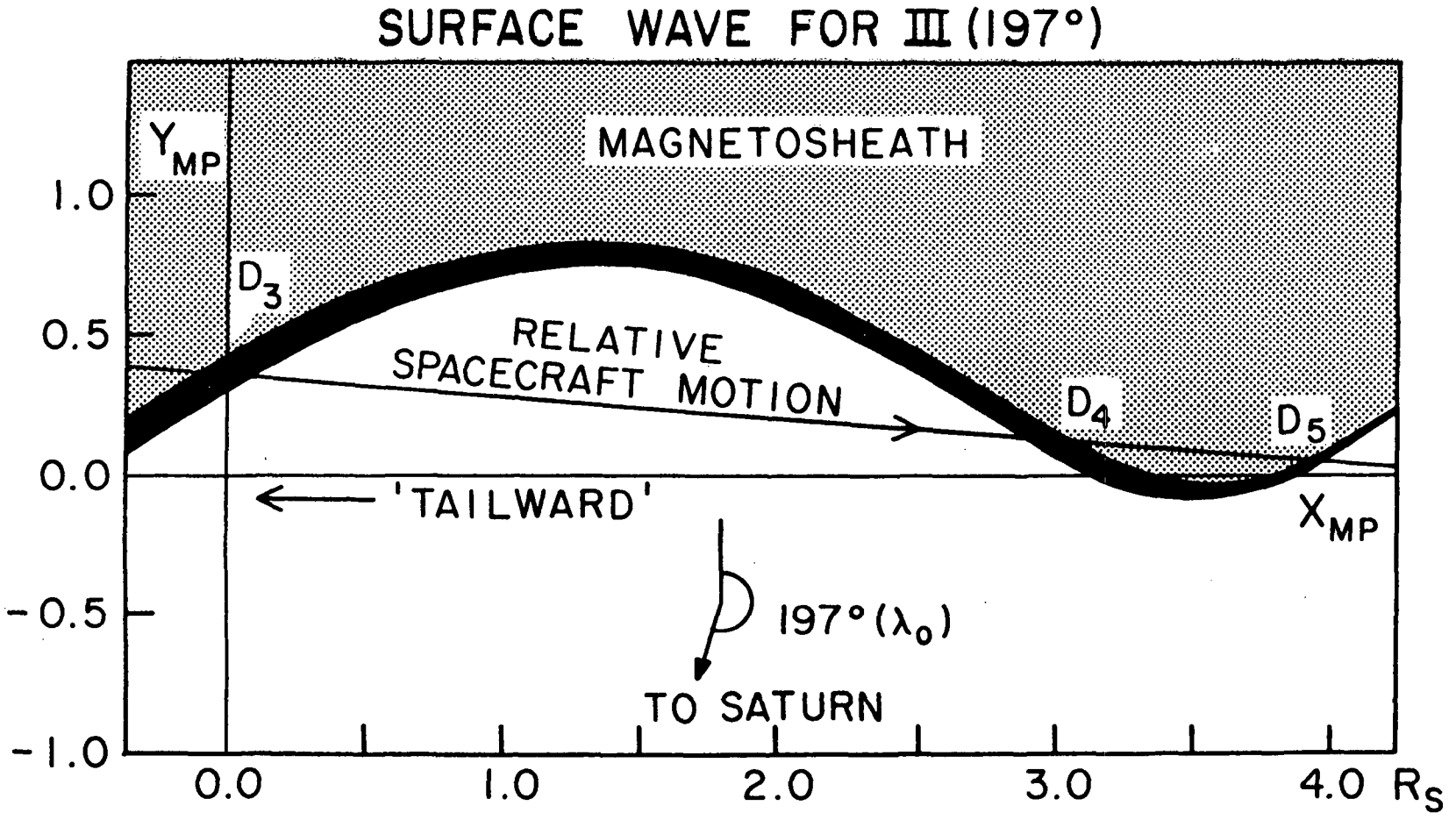
SURFACE WAVE FOR III (197°)
MAGNETOSHEATH
Y_{MP}
D_3
RELATIVE SPACECRAFT MOTION
D_4
D_5
'TAILWARD'
X_{MP}
197° (λ_o)
TO SATURN
1.0
0.5
0.0
-0.5
-1.0
0.0
1.0
2.0
3.0
4.0 R_S

FIGURE 20

Figure 21 Here we tabulate average characteristics of the "tailward" moving surface waves at Saturn from the analysis described above and compare them to those at Earth derived by a similar analysis (Lepping and Burlaga, 1979) also based on Voyager 1 data taken shortly after launch as the spacecraft left the Earth's dawnside MP. V_W is the phase speed (or group speed since zero dispersion is assumed) along the averaged position of the MP, A is the amplitude of the wave, λ is the wavelength, τ is the wave period, and d is an estimated MP thickness. Notice that both the amplitude and wavelength are approximately an order of magnitude larger at Saturn than at earth which is perhaps not surprising since the ratio of Saturn's subsolar point MP distance to Earth's is, on average (as observed), about 20, i.e., Saturn's magnetosphere is simply much larger (see Table 1 and Figure 4). Interestingly λ/A, which is well-determined, especially for Saturn, agrees nicely for the two planets to within a factor of about 2. Also interesting is the comparison of MP thicknesses at the two planets according to this method. Notice d_{MP} is about 10 times greater at Saturn than at earth. This agrees with the estimate of a probable ratio of proton gyroradii calculated for the MP at the two planets, if the B-field dominates the estimates, as expected, i.e., $B_{EARTH}/B_{SATURN} \sim 6$. As we see (footnote*), d_{MP} for Earth agrees well with determinations by Russell and Elphic (1978) from ISEE 1 and 2 MP crossings.

SURFACE WAVE CHARACTERISTICS

	SATURN	EARTH
V_W (KM/SEC)	180 (±90)	340 (+210/-95)
A (KM)	26 (±14)X10^3	2.1 (+3.8/-0.5)X10^3
λ (KM)	26 (±16)X10^4	4.7 (+3.0/-1.2)X10^4
λ/A	9.7 (±1.1)	23 (±4)
τ (MIN)	23 (±2)	2.8 (±1)
d_{MP} (KM)†	2,000 ↔ 8,000	300 ↔ 700*

† d_{MP} ≡ estimated thickness of MP

* Compare to Russell and Elphic (1978) results from ISEE 1 and 2 MP crossings for Local Time 1000 ↔ 1200: 500 ↔ 1000 KM.

FIGURE 21

SOME FUTURE STUDIES

- MAR'S OBSTACLE BOUNDARY: NATURE AND CHARACTERISTICS
- COMETS: S.W. INTERACTION GENERALLY (B.S., CD?, OTHER?)
- HIGH LATITUDE PORTIONS OF BOUNDARIES OF ALL PLANETS
- BS ASYMMETRY

FIGURE 22

Figure 22 In the last figure we suggest some areas which come to mind that are associated with bow shock and MP studies that are in very serious need of spacecraft observations and/or further analyses, especially the first two.

Acknowledgment I thank K. W. Behannon for reading the manuscript and making helpful comments.

References

Alpers, W., Steady state charge neutral models of the magnetopause, Astrophys. Space Sci., 5, 425, 1969.

Beard, D. B., The interactions of the solar wind with planetary magnetic fields: basic principles and obervations, Planet. Space Sci., 21, 1475, 1973.

Beard, D. B. and D. L. Jackson, The Jovian magnetic field and the magnetospheric shape, J. Geophys. Res., 81, 3399, 1976.

Behannon, K. W., Geometry of the geomagnetic tail, J. Geophys. Res., 75, 743, 1970.

Behannon, K. W., R. P. Lepping, and N. F. Ness, Structure and dynamics of Saturn's outer magnetosphere and boundary regions, J. Geophys. Res., 88, 8791, 1983.

Bridge, H. S., et al., Plasma observations near Saturn: Initial results from Voyager 1, Science, 212, 217, 1981.

Bridge, H. S., et al., Plasma observations near Saturn: Initial results from Voyager 2, Science, 215, 563, 1982.

Burlaga, L. F., Corotating pressure waves without streams, J. Geophys. Res., 88, 6085, 1983.

Cassen, P. and J. Szabo, The viscous magnetopause, Planet. Space Sci., 18, 349, 1970.

Choe, J. T., D. B. Beard, and E. C. Sullivan, Precise calculation of the magnetosphere surface for a tilted dipole, Planet. Space Sci., 21, 485, 1973.

Cloutier, P. A., Solar wind interaction with planetary ionospheres, Proceedings of seminar held at Moscow, U.S.S.R., Nov. 17-21, 1975, NASA-SP-397, 111, 1976.

Desch, M. D., Radio emission signature of Saturn's immersions in Jupiter's tail, J. Geophys. Res., 88, 6904, 1983.

Dryer, M., and G. R. Heckman, On the hypersonic analog as applied to planetary interaction with the solar wind, Planet. Space Sci., 15, 515, 1967.

Elphic, R. C. and C. T. Russell, ISEE-1 and 2 magnetopause observations: Magnetosheath magnetic field control of boundary motion and thickness, EOS Trans. AGU, 59, 1163, 1978.

Engle, I. and D. B. Beard, Idealized Jovian magnetosphere shape and field, J. Geophys. Res., 85, 579, 1980.

Fairfield, D. H., Average and unusual locations of the Earth's magnetopause and bow shock, J. Geophys. Res., 76, 6700, 1971.

Fairfield, D. H., Waves in the vicinity of the magnetopause, Proceedings of the Summer Advanced Study School on Magnetospheric Particles and Fields, Graz, Austria, 1975.

Fairfield, D. H., Structure of the magnetopause: observations and implications for reconnection, Space Sci. Rev., 23, 427, 1979.

Formisano, V., Orientation and shape of the Earth's bow shock in three dimensions, Plan. Space Sci., 27, 1151, 1979.

Formisano, V., V. Domingo, and K.-P. Wenzel, The three dimensional shape of the magnetopause, Planet. Space Sci., 27, 1137, 1979.

Grzedzielski, S., W. Macek, and P. Oberc, Expected immersion of Saturn's magnetosphere in the Jovian magnetic tail, Nature, 292, 615, 1981.

Holzer, R. E.,and J. A. Slavin, Magnetic flux transfer associated with expansions and contractions of the dayside magnetosphere, J. Geophys. Res., 83, 3831, 1978.

Ip, W.-H. and W. I. Axford, Theories of physical processes in the cometary comae and ion tails, Comets, ed. L. L. Wilkeining, The University of Arizona Press, Tucson, Arizona, 1982.

Kurth, W. S., J. D. Sullivan, D. A. Gurnett, F. L. Scarf, H. S. Bridge, and E. C. Sittler, Jr., Observations of Jupiter's distant magnetotail and wake, J. Geophys. Res., 87, 10373, 1982.

Lee, L. C., R. K. Albano, and J. R. Kan, Kelvin-Helmholtz instability in the magnetopause-boundary layer region, J. Geophys. Res., 86, 54, 1981.

Lepping, R. P. and L. F. Burlaga, Geomagnetopause surface fluctuations observed by Voyager 1, J. Geophys. Res., 84, 7099, 1979.

Lepping, R. P., N. F. Ness, and K. W. Behannon, Summary of Mariner 10 magnetic field and trajectory data for Mercury I and III encounters (and references therein), NASA TM-80600, Nov. 1979.

Lepping, R. P., L. F. Burlaga, and L. W. Klein, Surface waves on Saturn's magnetopause, Nature, 292, 750, 1981.

Lepping, R. P., L. F. Burlaga, L. W. Klein, J. M. Jessen, and C. C. Goodrich, Observations of the magnetic field an plasma flow in Jupiter's magnetosheath, J. Geophys. Res., 86, 8141, 1981.

Lepping, R. P., M. D. Desch, L. W. Klein, E. C. Sittler, Jr., J. D. Sullivan, W. S. Kurth, and K. W. Behannon, Structure and other properties of Jupiter's distant magnetotail, J. Geophys. Res., 88, 8801, 1983.

Michel, F. C., Magnetopause shapes: General solutions, J. Geophys. Res., 82, 5181, 1977.

Michel, F. C., and A. J. Dessler, Diffusive entry of solar flare particles into the geomagnetic tail, J. Geophys. Res., 75, 6061, 1970.

Ness, N. F., Interaction of the solar wind with the Moon, Astrophys. Space Sci., Libr, part II, 159, 1972.

Ness, N. F., ed., Solar-wind interaction with the planets Mercury, Venus, and Mars, Proceedings of seminar held at Moscow, U.S.S.R., Nov. 17-21, 1975, NASA SP-397, 1976.

Ness, N. F., M. H. Acuña, R. P. Lepping, J. E. P. Connerney, K. W. Behannon, L. F. Burlaga, and F. M. Neubauer, Magnetic field studies by Voyager 1: Preliminary results at Saturn, Science, 212, 211, 1981.

Ness, N. F., M. H. Acuña, K. W. Behannon, L. F. Burlaga, J. E. P. Connerney, R. P. Lepping, and F. M. Neubauer, Magnetic field studies by Voyager 2: Preliminary results at Saturn, Science, 215. 558. 1982a.

Ness, N. F., M. H. Acuña, K. W. Behannon, and F. M. Neubauer, The induced magnetosphere of Titan, J. Geophys. Res., 87, 1369, 1982b.

Olson, W. P., The geomagnetic field and its extension into space, Adv. Space Res., 2, 13, 1982.

Olson, W. P. and K. A. Pfitzer, Magnetospheric magnetic field modeling, McDonnel Douglas Astronautics Co., preprint, 1977.

Paschmann, G., Plasma structure of the magnetopause and boundary layer, Proceedings of Magnetospheric Boundary Layers Conference, Alpbach, 11-15 June 1979, (ESA SP-148, August, 1979).

Rizzi, A. W., Solar-wind flow past the planets earth, Mars, and Venus, Ph.D. Thesis, Stanford University, Stanford, CA, May 1971.

Romanov, S. A., V. N. Smirnov, and O. L. Vaisberg, Interaction of the solar wind with Venus, Cosmic Res., 16, 603, 1978.

Russell, C. T., R. C. Elphic, Initial ISEE magnetometer results: Magnetopause observations, Space Sci. Rev., 22, 681, 1978.

Russell, C. T., R. C. Elphic, and J. A. Slavin, Limits on the possible intrinsic magnetic field of Venus, J. Geophys. Res., 85, 8319, 1980. (See other papers in this issue related to Venus' bow shock and ionopause boundaries.)

Russell, C. T., J. G. Luhamnn, R. C. Elphic, and M. Neugebauer, Solar wind interaction with comets: Lessons from Venus, Comets, ed. L. L Wilkening, The University of Arizona Press, Tucson, Arizona, 1982.

Scarf, F. L., L. A. Frank, and R. P. Lepping, Magnetosphere boundary observations along the IMP-7 orbit: Part 1, boundary locations and wave level variations, J. Geophys. Res., 82, 5171, 1977.

Scarf, F. L., D. A. Gurnett, and W. S. Kurth, Plasma wave turbulence at planetary bow shocks, Nature, 292, 747, 1981.

Siscoe, G. L., Towards a comparitive theory of magnetospheres, Solar System

Plasma Physics, vol. 2, eds. C. F. Kennel, L. J. Lanzerotti, and E. N. Parker, North-Holland Pub. Co., Amsterdam, 1979.

Siscoe, G. L., N. U. Crooker, and J. W. Belcher, Sunward flow in Jupiter's magnetosheath, Geophys. Res. Lett., 7, 25, 1980.

Slavin, J. A., and R. E. Holzer, Solar wind flow about the terrestrial planets, 1, modeling bow shock position and shape, J. Geophys. Res., 86, 11401, 1981.

Slavin, J. A. and R. E. Holzer, The solar wind interaction with Mars revisited, J. Geophys. Res., 87, 10285, 1982.

Slavin, J. A., R. E. Holzer, J. R. Spreiter, S. S. Stahara, and D. S. Chaussee, Solar wind flow about the terrestrial planets 2. comparison with gas dynamic theory and implications for solar-planetary interactions, J. Geophys. Res., 88, 19, 1983.

Slavin, J. A., E. J. Smith, P. R. Gazis, and J. D. Mihalov, A Pioneer-Voyager study of the solar wind interaction with Saturn, Geophys. Res. Lett., 10, 9, 1983.

Spreiter, J. R., Magnetohydrodynamic and gasdynamic aspects of solar-wind flow around terrestrial planets: A critical review, Proceedings of seminar held at Moscow, U.S.S.R., Nov. 17-21, 1975, NASA SP-397, 135, 1976.

Spreiter, J. R., A. L. Summers, and A. Y. Alksne, Hydromagnetic flow around the Magnetosphere, Planet. Space Sci., 14, 223, 1966.

Spreiter, J. R., A. Y. Alksne, and A. L. Summers, External aerodynamics of the magnetosphere, NASA TN D-4482, June 1968.

Spreiter, J. R. and A. Y. Alksne, Plasma flow around the magnetosphere, Rev. Geophys., 7, 11, 1969.

Sprieter, J. R., and A. Y. Alksne, Solar wind flow past objects in the solar system, Annu. Rev. Fluid Mech., 2, 313, 1970.

Spreiter, J. R. and S. S. Stahara, A new predictive model for determining solar wind-terrestrial planet interactions, J. Geophys. Res., 85, 6769, 1980.

Stahara, S. S., D. Klenke, B. C. Trudinger, and J. R. Spreiter, Application of advanced computational procedures for modeling solar-wind interactions with Venus - theory and computer code, NASA, NEAR TR 202, (Nielsen Engineering & Research Inc., Mountain View, CA), October 1979.

Swift, D. W., and L. C. Lee, Rotational discontinuities and the structure of the magnetopause, J. Geophys. Res., 88, 111, 1983.

Tatrallyay, M., C. T. Russell, J. D. Mihalov, and A. Barnes, Factors controlling the location of the Venus bow shock, J. Geophys. Res., 88, 5613, 1983.

Vaisberg, O. L., A. V. Bogdanov, V. N. Smirnov, and S. A. Romanov, On the

nature of the solar-wind-Mars interaction, Proceedings of seminar held at Moscow, U.S.S.R., Nov. 17-21, 1975, NASA SP-397, 21, 1976.

Van Dyke, M. D., The supersonic blunt body problem - Review and extension, J. AeroSp. Sci., 29, 485, 1958.

Wallis, M. K. and M. Dryer, Sun and comets as sources in an external flow, Ap. J., 205, 895, 1976.

Wilkening, L. L., ed., Comets, The University of Arizona Press, Tucson, Arizona, 1982.

Willis, D. M., Structure of the magnetopause, Rev. Geophys. Space Phys., 9, 953, 1971.

Willis, D. M., The magnetopause: Microstructure and interaction with magnetospheric plasma, J. atmos. terr. Phys., 40, 301, 1978.

BIBLIOGRAPHIC DATA SHEET

1. Report No. TM 86114	2. Government Accession No.	3. Recipient's Catalog No.
4. Title and Subtitle A Comparative Review of Bow Shocks and Magnetopauses		5. Report Date
		6. Performing Organization Code 695
7. Author(s) R. P. Lepping		8. Performing Organization Report No.
9. Performing Organization Name and Address Planetary Magnetospheres Branch Laboratory for Extraterrestrial Physics Goddard Space Flight Center Greenbelt, Maryland 20771		10. Work Unit No.
		11. Contract or Grant No.
12. Sponsoring Agency Name and Address		13. Type of Report and Period Covered
		14. Sponsoring Agency Code
15. Supplementary Notes		

16. Abstract

This document is an expanded summary of a 30 minute review talk, originally entitled "Bow Shock and Magnetopauses Formation", presented at the Conference on Planetary Plasma Environmrnts: A Comparative View at Yosemite, California, on January 30 - February 3, 1984. This version is considerably extended generally in detail of discussion. It contains a highly selective number of topics presented with the intention of giving a broad overview of what is presently known. Figures 18, 20, and 22, not presented in the talk, have been added for completeness.

Not all of the references listed at the end of the document are cited in the text. Some were included simply to add to the usefulness and completeness of the list. For the sake of readibility, no references appear in the introduction.

17. Key Words (Selected by Author(s))		18. Distribution Statement	
19. Security Classif. (of this report) Unclassified	20. Security Classif. (of this page) Unclassified	21. No. of Pages 54	22. Price*

*For sale by the National Technical Information Service, Springfield, Virginia

22161

GSFC 25-44 (10/77)